CORONAVIRUS

Broadly neutralizing antibodies against sarbecoviruses generated by immunization of macaques with an AS03-adjuvanted COVID-19 vaccine

Yupeng Feng[1]†, Meng Yuan[2]†, John M. Powers[3]†, Mengyun Hu[1], Jennifer E. Munt[3], Prabhu S. Arunachalam[1], Sarah R. Leist[3], Lorenza Bellusci[4], JungHyun Kim[4], Kaitlin R. Sprouse[5], Lily E. Adams[3], Sumana Sundaramurthy[6], Xueyong Zhu[2], Lisa M. Shirreff[7], Michael L. Mallory[3], Trevor D. Scobey[3], Alberto Moreno[8], Derek T. O'Hagan[9], Harry Kleanthous[10], Francois J. Villinger[7], David Veesler[5,11], Neil P. King[5,12], Mehul S. Suthar[13], Surender Khurana[4], Ralph S. Baric[3]*, Ian A. Wilson[2]*, Bali Pulendran[1,14,15]*

The rapid emergence of severe acute respiratory syndrome coronavirus 2 (SARS-CoV-2) variants that evade immunity elicited by vaccination has placed an imperative on the development of countermeasures that provide broad protection against SARS-CoV-2 and related sarbecoviruses. Here, we identified extremely potent monoclonal antibodies (mAbs) that neutralized multiple sarbecoviruses from macaques vaccinated with AS03-adjuvanted monovalent subunit vaccines. Longitudinal analysis revealed progressive accumulation of somatic mutation in the immunoglobulin genes of antigen-specific memory B cells (MBCs) for at least 1 year after primary vaccination. Antibodies generated from these antigen-specific MBCs at 5 to 12 months after vaccination displayed greater potency and breadth relative to those identified at 1.4 months. Fifteen of the 338 (about 4.4%) antibodies isolated at 1.4 to 6 months after the primary vaccination showed potency against SARS-CoV-2 BA.1, despite the absence of serum BA.1 neutralization. 25F9 and 20A7 neutralized authentic clade 1 sarbecoviruses (SARS-CoV, WIV-1, SHC014, SARS-CoV-2 D614G, BA.1, and Pangolin-GD) and vesicular stomatitis virus–pseudotyped clade 3 sarbecoviruses (BtKY72 and PRD-0038). 20A7 and 27A12 showed potent neutralization against all SARS-CoV-2 variants and multiple Omicron sublineages, including BA.1, BA.2, BA.3, BA.4/5, BQ.1, BQ.1.1, and XBB. Crystallography studies revealed the molecular basis of broad and potent neutralization through targeting conserved sites within the RBD. Prophylactic protection of 25F9, 20A7, and 27A12 was confirmed in mice, and administration of 25F9 particularly provided complete protection against SARS-CoV-2, BA.1, SARS-CoV, and SHC014 challenge. These data underscore the extremely potent and broad activity of these mAbs against sarbecoviruses.

INTRODUCTION

The zoonotic spillover of coronaviruses has caused three outbreaks of severe respiratory diseases within the past 20 years (1–3). Severe acute respiratory syndrome coronavirus 2 (SARS-CoV-2), the virus that causes coronavirus disease 2019 (COVID-19), has caused an enormous global health crisis, with more than 759 million confirmed cases and more than 6.8 million deaths as of 7 March 2023. Although COVID-19 vaccines and therapeutic antibodies have been developed at unprecedented speed, a series of variants of concern have emerged since late 2020. The antigenically distant Omicron variant, first identified in Botswana in November 2021, has spread worldwide with multiple sublineages that evade neutralization by antibodies and has posed a serious challenge to current vaccination strategies (4–6). Recent studies have revealed that mRNA monovalent vaccine efficacy during the BA.4/5 waves was below 50% after two or three doses, with a fourth dose causing only a minimal, transient increase in Omicron-neutralizing antibodies (4–6). Furthermore, now-available therapeutic antibodies suffer from a loss of efficacy against Omicron variants (7, 8), urging the need for broadly protective vaccines (9) and monoclonal antibodies (mAbs).

We recently performed a study in macaques to benchmark clinically relevant adjuvants [including AS03, an α-tocopherol–containing oil-in-water emulsion; AS37, a Toll-like receptor 7 (TLR7) agonist adsorbed to alum; CpG1018-alum, a TLR9 agonist formulated in alum (CpG); Essai O/W 1849101, a squalene-in-water emulsion (OW); and Alum] for their capacity to enhance the protective immunity of SARS-CoV-2 vaccines, comprising either a SARS-CoV-2 receptor binding domain (RBD) or a prefusion-

[1]Institute for Immunity, Transplantation and Infection, Stanford University, Stanford, CA 94305, USA. [2]Department of Integrative Structural and Computational Biology, Scripps Research Institute, La Jolla, CA 92037, USA. [3]Department of Epidemiology, University of North Carolina at Chapel Hill, Chapel Hill, NC 27599, USA. [4]Division of Viral Products, Center for Biologics Evaluation and Research, Food and Drug Administration (FDA), Silver Spring, MD 20993, USA. [5]Department of Biochemistry, University of Washington, Seattle, WA 98195, USA. [6]Sino Biological US Inc., Wayne, PA 19087, USA. [7]New Iberia Research Center, University of Louisiana at Lafayette, New Iberia, LA 70560, USA. [8]Division of Infectious Diseases, Department of Medicine, Emory University School of Medicine, Atlanta, GA 30322, USA. [9]GSK, Rockville, MD 20850, USA. [10]Bill and Melinda Gates Foundation, Seattle, WA 98109, USA. [11]Howard Hughes Medical Institute, University of Washington, Seattle, WA 98195, USA. [12]Institute for Protein Design, University of Washington, Seattle, WA 98195, USA. [13]Department of Pediatrics, Emory Vaccine Center, Emory National Primate Research Center, Atlanta, GA 30329, USA. [14]Department of Pathology, Stanford University School of Medicine, Stanford University, Stanford, CA 94305, USA. [15]Department of Microbiology and Immunology, Stanford University School of Medicine, Stanford, CA 94305, USA.
*Corresponding author. Email: bpulend@stanford.edu (B.P.); wilson@scripps.edu (I.A.W.); rbaric@email.unc.edu (R.S.B.)
†These authors contributed equally to this work.

stabilized spike protein (Hexapro) on the surface of a self-assembling nanoparticle (NP) (10). We subsequently showed that a booster with RBD (beta)–NP, comprising the SARS-CoV-2 beta variant RBD, 1 year later elicited robust heterotypic protection against Omicron in macaques (11). Here, we analyzed banked samples from this study to investigate the evolution of the memory B cell (MBC) response at the monoclonal level over a period of 1.5 years in rhesus macaques receiving the AS03-adjuvanted subunit vaccine. We observed increased neutralization potency and breadth of mAbs isolated 6 to 12 months after the primary vaccination (the first two-dose vaccination) and 3 weeks to 6 months after the booster (the third dose vaccination at 12 months). Furthermore, we performed a serological assessment of the 15 most potent mAbs isolated 3 weeks to 6 months after the primary vaccination, performed a detailed structural analysis of a subset of these antibodies, and demonstrated their efficacy in protecting against Omicron variants of SARS-CoV-2 and other sarbecoviruses infections in mice.

RESULTS
AS03-adjuvanted RBD-NP/Hexapro-NP vaccination elicits progressive MBC maturation
We analyzed the antigen-specific, MBC responses from banked peripheral blood mononuclear cell (PBMC) samples from our previous study (10), in which rhesus macaques were immunized with RBD-NP adjuvanted with alum, OW, AS37, CpG, or AS03 (fig. S1A). We enumerated the circulating SARS-CoV-2 RBD–specific immunoglobulin G–positive (IgG$^+$) MBCs by flow cytometry using fluorescent-labeled probes (fig. S1B). The MBC frequency, variable (V) gene somatic hypermutation (SHM), and complementarity-determining region (CDR) 3 length were comparable among groups (fig. S1, C to E), suggesting that vaccination with these five different adjuvants exhibited a similar pattern of antigen-specific MBC responses.

In addition, we analyzed MBC responses using banked PBMC samples from our recent study (11), in which macaques were immunized with a two-dose primary vaccination of AS03-adjuvanted RBD-NP ($n = 5$) or Hexapro-NP ($n = 6$) at days 0 and 21, followed by a booster vaccination with AS03-adjuvanted RBD (beta)–NP 1 year later (Fig. 1A). We assessed the kinetics of the antibody response and MBCs in blood over 1.5 years in animals immunized with RBD-NP-AS03 or Hexapro-NP-AS03. Vaccination induced potent and broadly neutralizing antibodies (bnAbs) against SARS-CoV-2 and Omicron variants after the booster (Fig. 1B and fig. S1, F and G). Omicron neutralizing antibodies were not detectable at 5 to 6 months after primary immunization, as described in our previous report (11, 12). We used flow cytometry to enumerate antigen-specific (RBD$^+$ for the RBD-NP group and Spike$^+$ for the Hexapro-NP group) MBCs in the blood (Fig. 1C and fig. S1B). The frequency of antigen-specific IgG$^+$ MBCs peaked at 1.4 months and declined over the next 5 to 6 months after vaccination (Fig. 1D and fig. S2A). Immunization with Hexapro-NP elicited a high proportion of IgG$^+$ MBCs targeting the non-RBD region of the spike protein, although there was no difference in RBD-specific IgG$^+$ MBCs between RBD-NP and Hexapro-NP (Fig. 1D).

Next, we analyzed the degree of SHM using the international ImMunoGeneTics information system (IMGT) database (13) in the V genes of both heavy and light chains of antigen-specific MBCs and observed a progressive increase in the frequency of SHM from 1.4

months to 5 to 6 months, plateauing at 12 months (Fig. 1, E and F). Booster immunization did not drive a further increase in SHM (Fig. 1, E and F). Using a more comprehensive rhesus macaque Ig gene database, the Karolinska Macaque database (KIMDB) (14), we similarly observed that the degree of SHM increased over time (fig. S2B). To determine the germline gene usage of anti–SARS-CoV-2 antibodies in macaques, we compared V gene nucleotide sequences of SARS-CoV-2 spike protein–specific MBCs with the *Macaca mulatta* Ig set from the IMGT database and the KIMDB database using IgBLAST. Analyses showed that *VH4-122* (IMGT) and *VH4-93* (KIMDB) were the most abundant (fig. S2, C and D). The closest germline gene of rhesus macaque *VH4-122* in humans is *VH4-59* (fig. S2E), a highly represented germline gene encoding anti–SARS-CoV-2 antibodies (15). In humans, *VH3-53* is one of the most frequently represented genes encoding antibodies generated in response to SARS-CoV-2 infection or mRNA vaccination. The structural basis of antibodies encoded by *VH3-53* has been extensively studied and showed a highly convergent binding approach to the receptor binding site (RBS) (15–17). The corresponding germline genes in rhesus macaque that are most similar to *VH3-53* are *VH3-103* (91.1%), *VH3-100* (89.9%), and *VH3S42* (89.9%), all of which have the SGGS motif in CDRH2 but no NY motif in CDRH1 (fig. S2E). Furthermore, those human *VH3-53*–like germline genes were also abundantly represented in rhesus macaques (fig. S2B).

Maturation of the B cell response generates antibodies with greater potency and breadth
To assess the evolution of the antibody repertoire encoded in antigen-specific MBCs, we sorted 3788 single SARS-CoV-2 Wuhan spike protein–specific IgG$^+$ MBCs at indicated time points from macaques from all groups (RBD-NP plus all adjuvants and Hexapro-NP-AS03) (Fig. 1A and fig. S1A), isolated 514 mAbs, and assessed their binding and neutralization potential (Fig. 2A). Consistent with the indistinguishable SHM and CDR3 amino acid lengths (fig. S1, D and E), mAbs isolated from animals from the different adjuvanted groups displayed similar binding profiles (fig. S3A). Henceforth, all 514 mAbs were grouped per time for antibody evolution analysis.

In total, 427 of the 514 (about 83.1%) mAbs bound to the SARS-CoV-2 Wuhan spike protein measured by enzyme-linked immunosorbent assay (ELISA), and the binding capacities (area under curve) correlated weakly but significantly ($r = 0.32$, $P < 0.0001$) with the heavy-chain SHM (fig. S3B). As expected, binding increased over time after the primary vaccination and plateaued at 12 months (fig. S3C). We further assayed the cross-reactivities of those mAbs against BA.1 and BA.4/5 by ELISA (fig. S4A). The correlation between Omicron binding and SHM was absent (fig. S4, B to E). However, the proportion of wild-type, BA.1, and BA.4/5 triple-reactive mAbs increased over time and peaked at 12 months (fig. S4F).

Next, we selected the top 206 BA.1 binding mAbs for neutralization screening against pseudotyped SARS-CoV-2 Wuhan, BA.1, and BA.4/5 strains. Of the 206 mAbs, 83.5% neutralized SARS-CoV-2 Wuhan, whereas 68.45 and 57.77% neutralized BA.1 and BA.4/5, respectively (Fig. 2B). The average potency of neutralizing antibodies against BA.1 or BA.4/5 was also significantly ($P < 0.05$ or $P < 0.0001$, respectively) lower than against the Wuhan strain, reflecting the fact that the vaccine contained the Wuhan strain

Feng *et al.*, *Sci. Transl. Med.* **15**, eadg7404 (2023)   10 May 2023

2 of 13
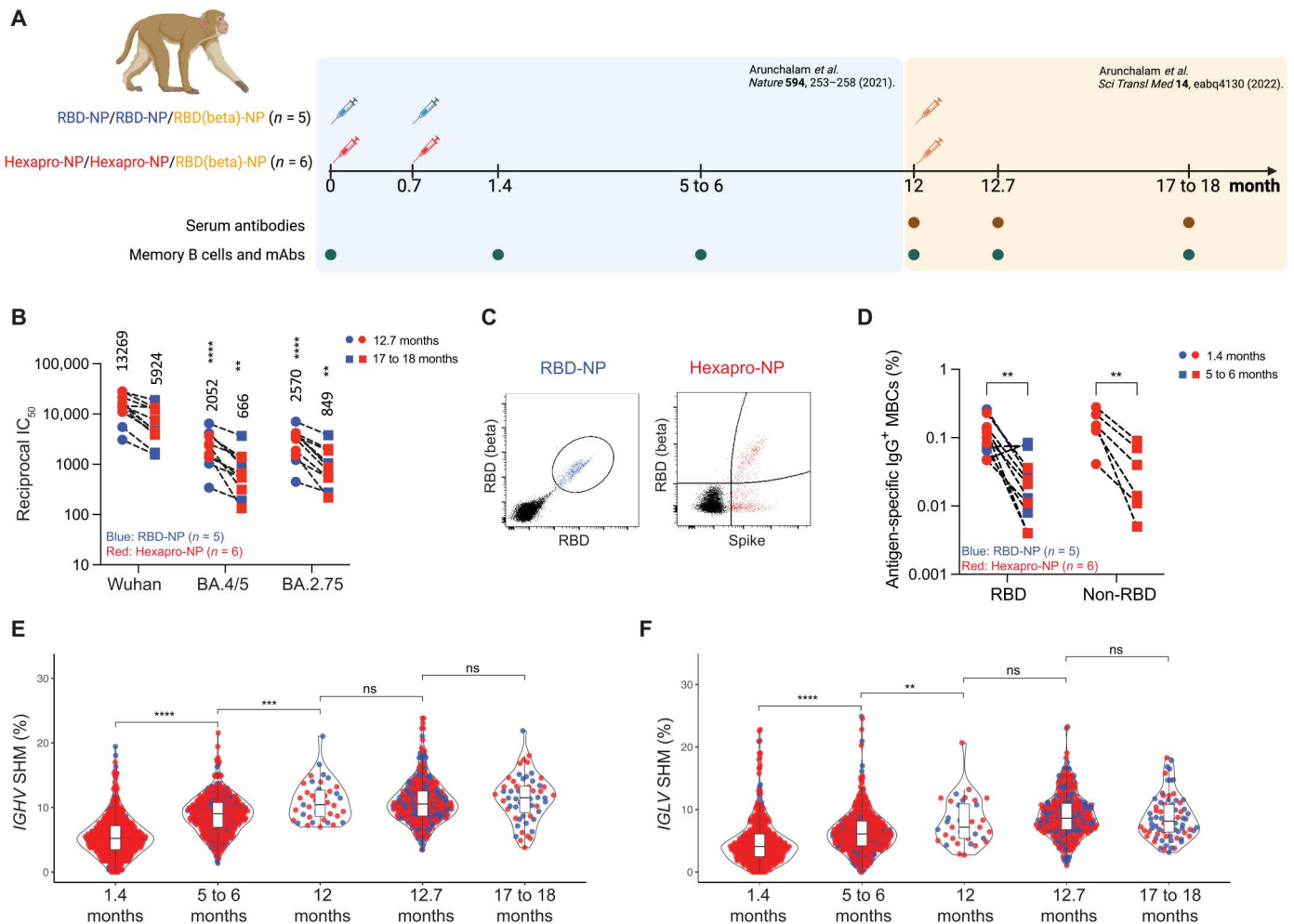
Fig. 1. AS03-adjuvanted RBD-NP/Hexapro-NP vaccination elicits progressive MBC maturation. (**A**) Study overview. Rhesus macaques received AS03-adjuvanted RBD-NP or Hexapro-NP on days 0 and 21 and received a booster with RBD (beta)–NP with AS03 at 12 months. Analysis of banked blood samples was performed as illustrated in the diagram. (**B**) Pseudovirus neutralizing antibody responses against viruses indicated on the x axis are shown. Each symbol represents an animal [RBD-NP (blue; n = 5) and Hexapro-NP (red; n = 6)], and paired samples are connected with a dashed line. The numbers within the graphs show geometric mean titers. The statistical differences were calculated using two-way ANOVA, and the statistical differences between indicated viruses and the SARS-CoV-2 Wuhan strain at the same time points are labeled as (**$P < 0.01$ and ****$P < 0.0001$). (**C**) Representative flow cytometry plots show dual RBD and RBD (beta)–binding B cells for RBD-NP vaccinated animals (blue) and dual spike protein and RBD (beta)–binding B cells for Hexapro-NP–vaccinated animals (red). Cells were pregated on live, $CD3^-$ $CD14^-$ $CD16^-$ $CD20^+$ IgD^- IgM^- IgG^+ B cells. (**D**) The frequency of antigen-specific IgG^+ MBCs relative to $CD20^+$ B cells is shown for samples from the RBD-NP (blue) and Hexapro-NP (red) groups. The binding region is indicated on the x axis. The statistical differences were calculated using two-way ANOVA (**$P < 0.01$). (**E** and **F**) Shown are the somatic hypermutation (SHM) rates of the productive *IGHV* genes (E) and *IGLV* genes (F) of B cells isolated from RBD-NP (blue)– or Hexapro-NP (red)–vaccinated animals at indicated time points. In (E) and (F), the boxes inside the violin plot show median, upper, and lower quartiles. The whiskers represent minimum and maximum values. Each dot represents an individual gene. The statistical differences between time points were calculated using one-way ANOVA [not significant (ns) > 0.05, **$P < 0.01$, ***$P < 0.001$, and ****$P < 0.0001$].

(Fig. 2B). To determine whether antibody maturation in binding and cross-reactivity translated into enhanced neutralizing potency and breadth, we analyzed the neutralization profiles as a function of time after immunization. There was an increase ($P < 0.05$) in the frequency of SARS-CoV-2 Wuhan, BA.1, and BA.4/5 triple-neutralizing antibodies, and a decrease in the percentage of nonneutralizing antibodies over 1.5 years, an indication of the evolution in the neutralization potency and breadth (Fig. 2C). Further examining the consequence of this evolution, we found that the average potency of neutralization against SARS-CoV-2 Wuhan and BA.1 was significantly ($P < 0.001$) improved by the booster (Fig. 2D).
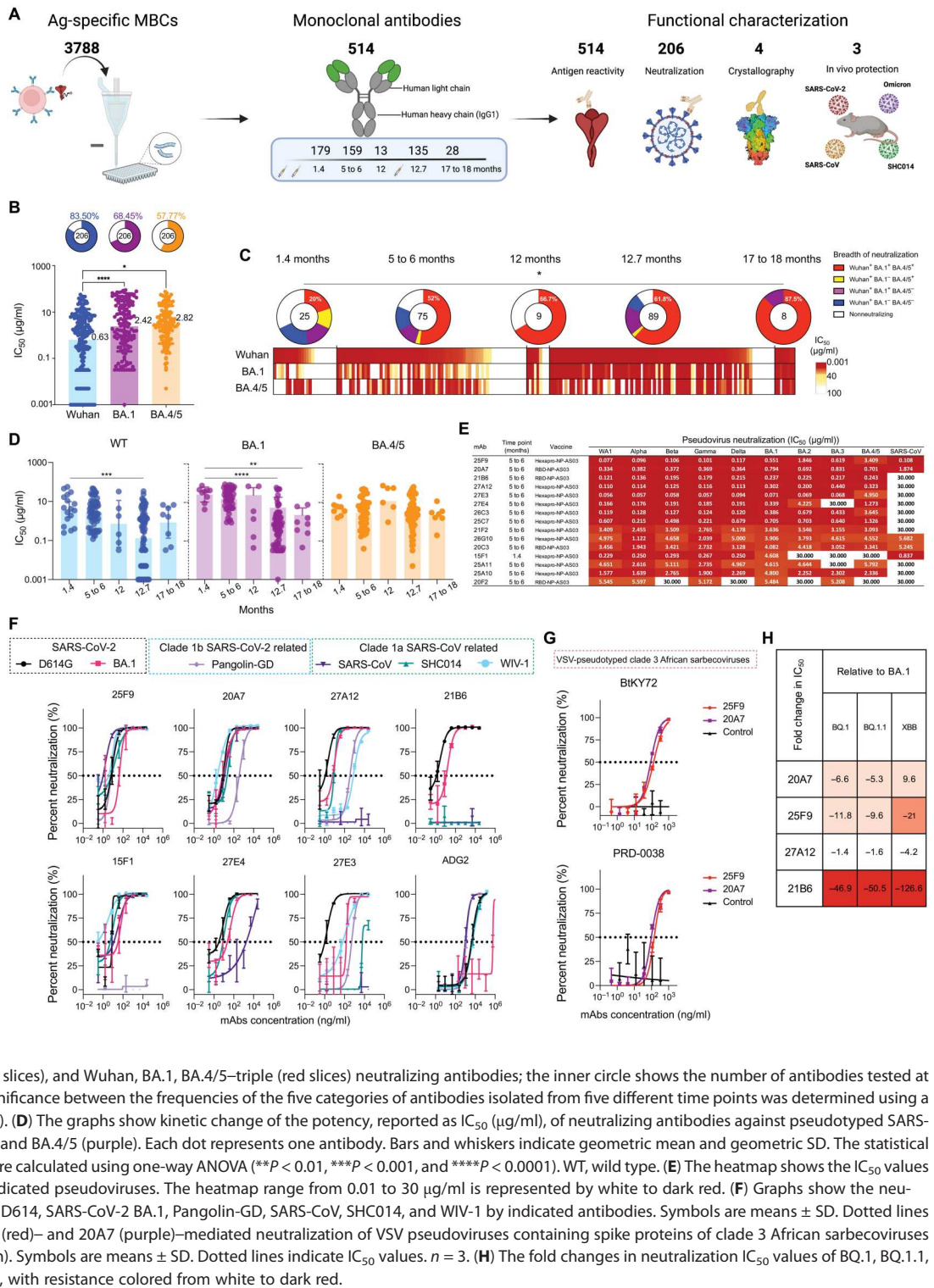
Collectively, our data demonstrate an evolution of mAbs in the MBC compartment toward higher neutralization potency and breadth.

Potent bnAbs show pan-sarbecovirus breadth

To identify SARS-CoV-2 bnAbs, we further characterized the neutralizing antibodies isolated at 1.4 months and 5 to 6 months and identified 15 mAbs showing better or comparable neutralizing activity against the BA.1 variant in a side-by-side comparison assay with a recently described BA.1 neutralizing antibody, S2H97 (fig. S5A) (*18*). All 15 mAbs displayed high avidities [apparent

Fig. 2. Maturation of the B cell response generates antibodies with greater potency and breadth. (**A**) Diagram depicting the strategy for antigen (Ag)–specific MBC sorting, mAb isolation, and characterization. (**B**) Graphs showing the neutralizing activity of monoclonal antibodies measured by pseudovirus neutralization assays. Bar graphs show IC_{50} values of all neutralizing antibodies against SARS-CoV-2 Wuhan (blue), BA.1 (purple), and BA.4/5 (orange) pseudoviruses. Each dot represents one antibody. Pie charts illustrate the fraction of nonneutralizing (no valid IC_{50} or $IC_{50} > 100$ μg/ml) antibodies (white slices); the inner circles show the number of antibodies tested. The frequency of neutralizing antibodies against SARS-CoV-2 Wuhan (blue slices), BA.1 (purple slices), or BA.4/5 (orange slices) pseudoviruses is shown on top of each pie chart. Bars and whiskers indicate geometric mean and geometric SD. Statistical significance was determined by the two-tailed Kruskal-Wallis test with subsequent Dunn's multiple comparisons test (*$P < 0.05$ and ****$P < 0.0001$). (**C**) Heatmap shows the neutralization activity of mAbs isolated at indicated time points against pseudotyped SARS-CoV-2 Wuhan, BA.1, and BA.4/5. Each unit within the heatmap represents one antibody. The color gradient indicates IC_{50} values ranging from 0.001 (red) to 100 (white). Pie charts illustrate the fraction of nonneutralizers (white slices), SARS-CoV-2 Wuhan-only (blue slices), Wuhan and BA.1–double (purple slices),

Wuhan and BA.4/5–double (orange slices), and Wuhan, BA.1, BA.4/5–triple (red slices) neutralizing antibodies; the inner circle shows the number of antibodies tested at indicated time points. Statistical significance between the frequencies of the five categories of antibodies isolated from five different time points was determined using a two-tailed chi-square test (*$P < 0.05$). (**D**) The graphs show kinetic change of the potency, reported as IC_{50} (μg/ml), of neutralizing antibodies against pseudotyped SARS-CoV-2 Wuhan (blue), BA.1 (orange), and BA.4/5 (purple). Each dot represents one antibody. Bars and whiskers indicate geometric mean and geometric SD. The statistical differences between time points were calculated using one-way ANOVA (**$P < 0.01$, ***$P < 0.001$, and ****$P < 0.0001$). WT, wild type. (**E**) The heatmap shows the IC_{50} values of 15 selected mAbs against the indicated pseudoviruses. The heatmap range from 0.01 to 30 μg/ml is represented by white to dark red. (**F**) Graphs show the neutralization of authentic SARS-CoV-2 D614, SARS-CoV-2 BA.1, Pangolin-GD, SARS-CoV, SHC014, and WIV-1 by indicated antibodies. Symbols are means ± SD. Dotted lines indicate IC_{50} values. $n = 4$. (**G**) 25F9 (red)– and 20A7 (purple)–mediated neutralization of VSV pseudoviruses containing spike proteins of clade 3 African sarbecoviruses BtKY72 (top) and PRD-0038 (bottom). Symbols are means ± SD. Dotted lines indicate IC_{50} values. $n = 3$. (**H**) The fold changes in neutralization IC_{50} values of BQ.1, BQ.1.1, and XBB relative to BA.1 are shown, with resistance colored from white to dark red.

dissociation constant (K_d) < 0.1 nM] against RBDs of different SARS-CoV-2 variants of concern, and eight mAbs showed strong avidities (K_d < 0.1 to 12.4 nM) to the spike protein of SARS-CoV (Table 1). The breadth of these 15 BA.1 neutralizing antibodies was confirmed by neutralization of a panel of pseudoviruses carrying spike proteins of SARS-CoV-2 WA1, Alpha, Beta, Gamma, Delta, BA.1, BA.2, BA.3, BA.4/5, and SARS-CoV (fig. S5, B and C). Five bnAbs (25F9, 20A7, 21B6, 27A12, and 27E3) stood out for their little neutralization changes across the SARS-CoV-2 variants (Fig. 2E). 20A7 can neutralize all SARS-CoV-2 Omicron variants and SARS-CoV with little to no reduced potency as compared with SARS-CoV-2 WA1 (Fig. 2E).

We next evaluated the neutralization of authentic SARS-CoV-2 D614G, BA.1, Pangolin-GD-CoV, SARS-CoV, SHC014, WIV-1, and Middle East respiratory syndrome coronavirus (MERS-CoV) by seven bnAbs (25F9, 20A7, 21B6, 27A12, 27E3, 27E4, and 15F1) and a previously described ultrapotent bnAb, ADG2 (*19*). 25F9 neutralized all of the above SARS-related viruses with half-maximal inhibitory concentration (IC_{50}) values of 6, 42, 6, 0.85, 3, and 6 ng/ml, respectively, with potencies surpassing that observed with ADG2 in a head-to-head comparison (Fig. 2F and fig. S5C). 20A7 displayed similar neutralizing breadth as compared to 25F9, although there was a reduction of neutralization against Pangolin-GD, whereas none neutralized MERS-CoV (fig. S5C). Furthermore, 25F9 and 20A7 displayed neutralization against vesicular stomatitis virus (VSV)–pseudotyped clade 3 sarbecoviruses (Fig. 2G and fig. S5C) BtKY72 and PRD-0038 that were considered to have spillover

potential (*20*). 21B6 and 27A12 neutralized BA.1 with IC_{50} values of 11 and 5 ng/ml, respectively (Fig. 2F and fig. S5C). During the conduction of the study, new variants of concern, such as BQ.1.1 and XBB, become the dominant viruses. We assayed 25F9, 20A7, 27A12, and 21B6 for their neutralization against pseudotyped BQ.1, BQ.1.1, and XBB (Fig. 2H and fig. S5C). 27A12 exhibited comparable neutralization potencies against BQ.1, BQ.1.1, and XBB compared to that against BA.1 (Fig. 2H). 20A7 and 25F9 showed some reduction (Fig. 2H). However, their high authentic BA.1 neutralization potencies (6 and 42 ng/ml, respectively) (fig. S5C) make 20A7 and 25F9 competitive to recently described antibodies (*7*). Together, our data revealed the cellular and molecular basis of vaccine-induced antibody evolution. We isolated some extremely potent bnAbs (21B6, 27A12, 25F9, and 20A7) after the primary vaccination with an AS03-adjuvanted nanoparticle immunogen.

Potent bnAbs target conserved sites within the RBD
To define the epitopes of the bnAbs and the structural basis of their neutralization breadth, we performed competitive binding experiments using antibodies (CR3022, CC12.3, CV07-270, S2X259, and S2M11) whose epitopes are well characterized (*15, 21–24*). The top three potent Omicron neutralizers (27A12, 27E3, and 21B6) competed with the ultrapotent mAb, S2M11 (*24*), which recognizes an epitope overlapping with the RBS (fig. S6, A and B). Co-incubation of the top four antibodies with the greatest neutralization breadth (25F9, 20A7, 15F1, and 27E4) with CR3022 (*15*), a SARS-CoV neutralizing antibody, or with S2X259 (*23*), a pan-sarbecovirus neutralizing antibody, showed strong competition (83 to 96%), suggesting some similarity in their epitopes (fig. S6, A and B).

Next, we determined crystal structures of the SARS-CoV-2 RBD in complex with three antibodies isolated in this study (table S1): 25F9 (Fig. 3), 20A7 (Fig. 4), and 21B6 (fig. S7). Relative positions of epitopes of the three antibodies and the RBS, the CR3022 site, and the S309 (*25*) site are shown in Fig. 3A. 25F9 targets one side of the RBD with some overlap with the conserved CR3022 site (Fig. 3B), where about 80% of the 25F9 epitope is buried by the heavy chain (Fig. 3C). Heavy-chain (H) and light-chain (L) CDRs H2, H3, L1, and L3 and light-chain framework region 3 (LFR3) interact with the RBD (Fig. 3D). 25F9 binding clashes with the human angiotensin-converting enzyme 2 (ACE2) (Fig. 3E), which explains its high potency. 25F9 targets a conserved region of the RBD, where 23 to 27 of the 28 epitope residues are conserved among SARS-CoV-2 variants, including BQ.1.1 and XBB.1.5, and other SARS-like viruses, such as SARS-CoV (SARS1), Pang17, and RaTG13 (Fig. 3F), which further explains the high potency of 25F9 against a broad range of SARS-like viruses (Fig. 2, E and F). 25F9 V_H (variable region of Ig heavy chain) F54 inserts into a hydrophobic pocket in the RBD and stacks with aromatic residues RBD-Y365, F377, Y369, and P384 and aliphatic residue L387 (Fig. 3G). 25F9-V_H K52 side chain and V_H A52c backbone carbonyl hydrogen bond with RBD-Y369 side-chain hydroxyl and C379 backbone amide, respectively (Fig. 3G). The CDR H3 and light chain of 25F9 also form polar and hydrophobic interactions with the RBD (Fig. 3, H and I).

21B6 neutralizes a broad range of SARS-CoV-2 variants, including BA.2 and BA.5, with high potency, but does not neutralize other SARS-like viruses SARS-CoV and SHC014 (Fig. 2, E and F). In contrast, 21B6 binds the opposite side (above the S309 epitope) of the SARS-CoV-2 RBD (fig. S7A). Like 25F9, 21B6 targets the RBD with

Table 1. Binding avidities of indicated mAbs against RBDs of SARS-CoV-2 wild-type (WT), Omicron BA.1, Alpha, Beta, and Delta variants and spike proteins of SARS-CoV. n.a., not applicable; n.b., no binding.

mAb	Binding avidities measured by biolayer interferometry (apparent K_d, nM)					
	RBD (WT)	RBD (BA.1)	RBD (Alpha)	RBD (Beta)	RBD (Delta)	Spike (SARS-CoV)
25F9	<0.1	<0.1	<0.1	<0.1	<0.1	<0.1
20A7	<0.1	<0.1	<0.1	<0.1	<0.1	9.4
21B6	<0.1	<0.1	<0.1	<0.1	4.1	n.a.
27A12	<0.1	0.3	<0.1	<0.1	<0.1	n.a.
27E3	<0.1	14.4	<0.1	18.9	<0.1	n.a.
27E4	<0.1	<0.1	<0.1	<0.1	<0.1	12.4
26C3	<0.1	11.4	<0.1	2.0	<0.1	n.a.
25C7	<0.1	<0.1	<0.1	<0.1	<0.1	1.6
21F2	<0.1	<0.1	<0.1	<0.1	<0.1	n.a.
26G10	<0.1	<0.1	<0.1	<0.1	<0.1	0.6
20C3	<0.1	<0.1	<0.1	<0.1	<0.1	1.0
15F1	1.0	<0.1	<0.1	<0.1	<0.1	6.4
25A11	<0.1	<0.1	<0.1	<0.1	<0.1	n.a.
25A10	<0.1	<0.1	<0.1	<0.1	<0.1	n.a.
20F2	0.1	<0.1	<0.1	<0.1	<0.1	3.4
CR3022	14.1	17.4	12.0	12.7	8.3	n.a.
CC12.3	5.8	n.b.	n.a.	n.a.	n.a.	n.a.

Feng *et al.*, *Sci. Transl. Med.* **15**, eadg7404 (2023)   10 May 2023

5 of 13

Fig. 3. 25F9 recognizes a conserved region on the SARS-CoV-2 RBD. The SARS-CoV-2 RBD is shown in white, and human ACE2 is in pale green throughout all the figures; the heavy and light chains of 25F9 are in blue and lavender, respectively. For clarity, only variable domains of the antibodies are shown in all figures. (**A**) The relative locations of epitopes on the SARS-CoV-2 RBD (white). The RBS is shown in pale green, the CR3022 site is shown in yellow, and the S309 site is shown in pink. Epitopes of 25F9, 20A7, and 21B6 are highlighted in blue, orange, and red outlines, respectively. RBS and epitope residues are defined as buried surface area (BSA > 0 Å²) as calculated by Proteins, Interfaces, Structures and Assemblies (PISA; www.ebi.ac.uk/pdbe/prot_int/pistart.html). (**B**) The crystal structure of 25F9 in complex with the SARS-CoV-2 RBD. (**C**) The surface area of SARS-CoV-2 buried by the heavy and light chains (HC and LC, respectively) of 25F9. (**D**) 25F9 interacts with the RBD using CDRs H2, H3, L1, and L3 as well as LFR3. (**E**) The SARS-CoV-2 RBD with 25F9 super-imposed onto an RBD-ACE2 complex structure (PDB 6M0J) shows that 25F9 would clash (indicated with a red circle) with receptor ACE2. (**F**) Sequence alignment of epitope residues in a subset of SARS-like viruses. Residues that differ from wild-type SARS-CoV-2 are indicated in red. SARS2, wild-type SARS-CoV-2; SARS1, SARS-CoV-1. (**G** to **I**) Molecular interactions between the RBD and CDR H2 (G), CDR H3 (H), and light chain (I) are shown. Hydrogen bonds and salt bridges are indicated by dashed lines.
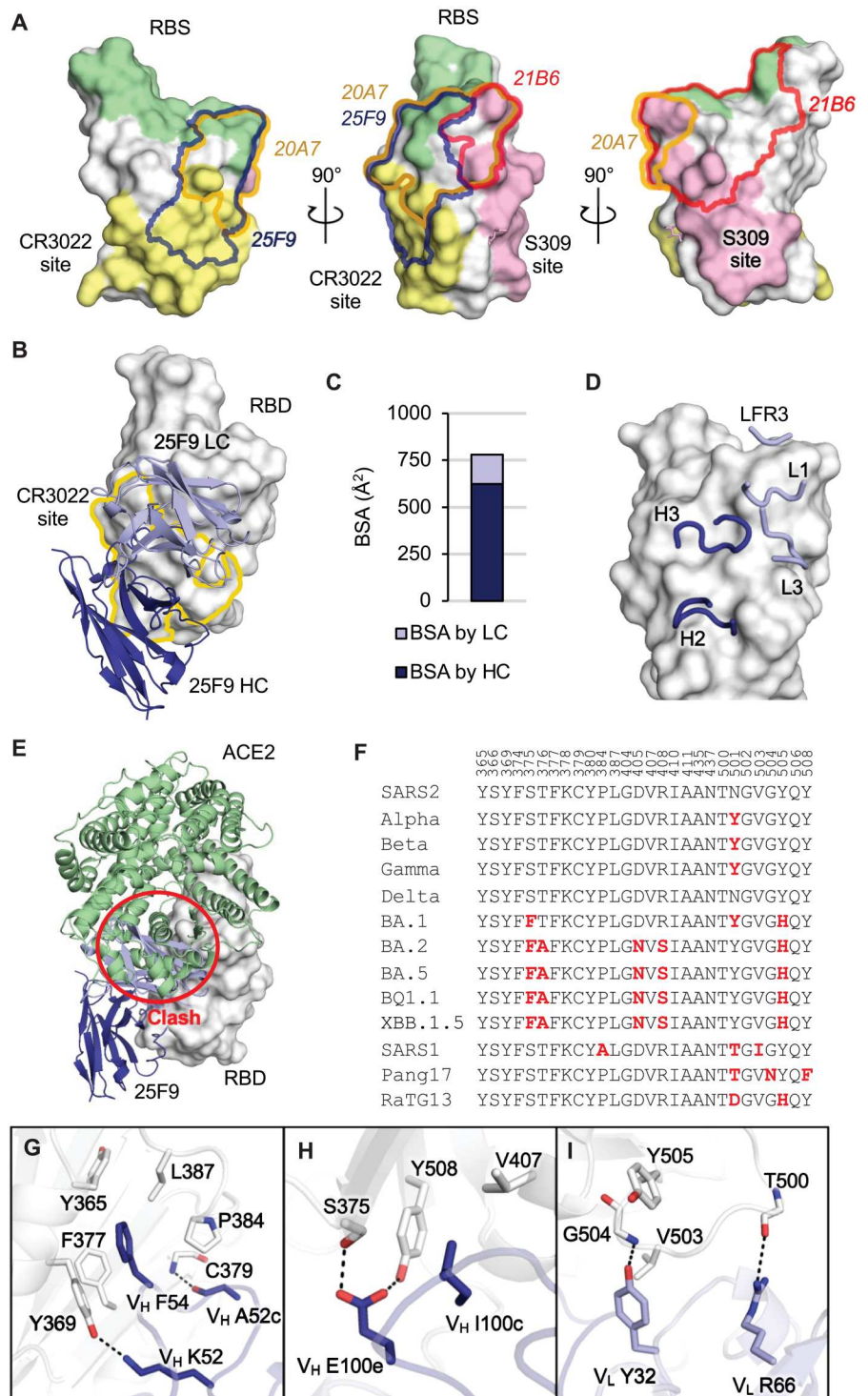
about 80% of its epitope area buried by the heavy chain (fig. S7B), and CDRs H1, H2, H3, and L2 and heavy-chain framework region 1 interact with the RBD (fig. S7C). 21B6 also clashes with ACE2 (fig. S7D). The 21B6 epitope residues are conserved from wild-type SARS-CoV-2 through Omicron subvariants BA.2 and BA.5 but vary in other SARS-like viruses (fig. S7E). RBD-Y351 hydrogen bonds with 21B6-V_H S30 and D31 and make hydrophobic

interactions with V_H T28 and Y32 (fig. S7F). CDR H2, especially V_H V52b and L52c, extensively interacts with a hydrophobic patch on the RBD formed by L452, Y351, L492, F490, and T470 (fig. S7G). CDR H3 and the light chain of 21B6 also form extensive interactions with the RBD (fig. S7, H and I). The R346T mutation in the most recent circulating Omicron subvariants BQ.1.1 and

Feng *et al.*, *Sci. Transl. Med.* **15**, eadg7404 (2023)   10 May 2023

6 of 13
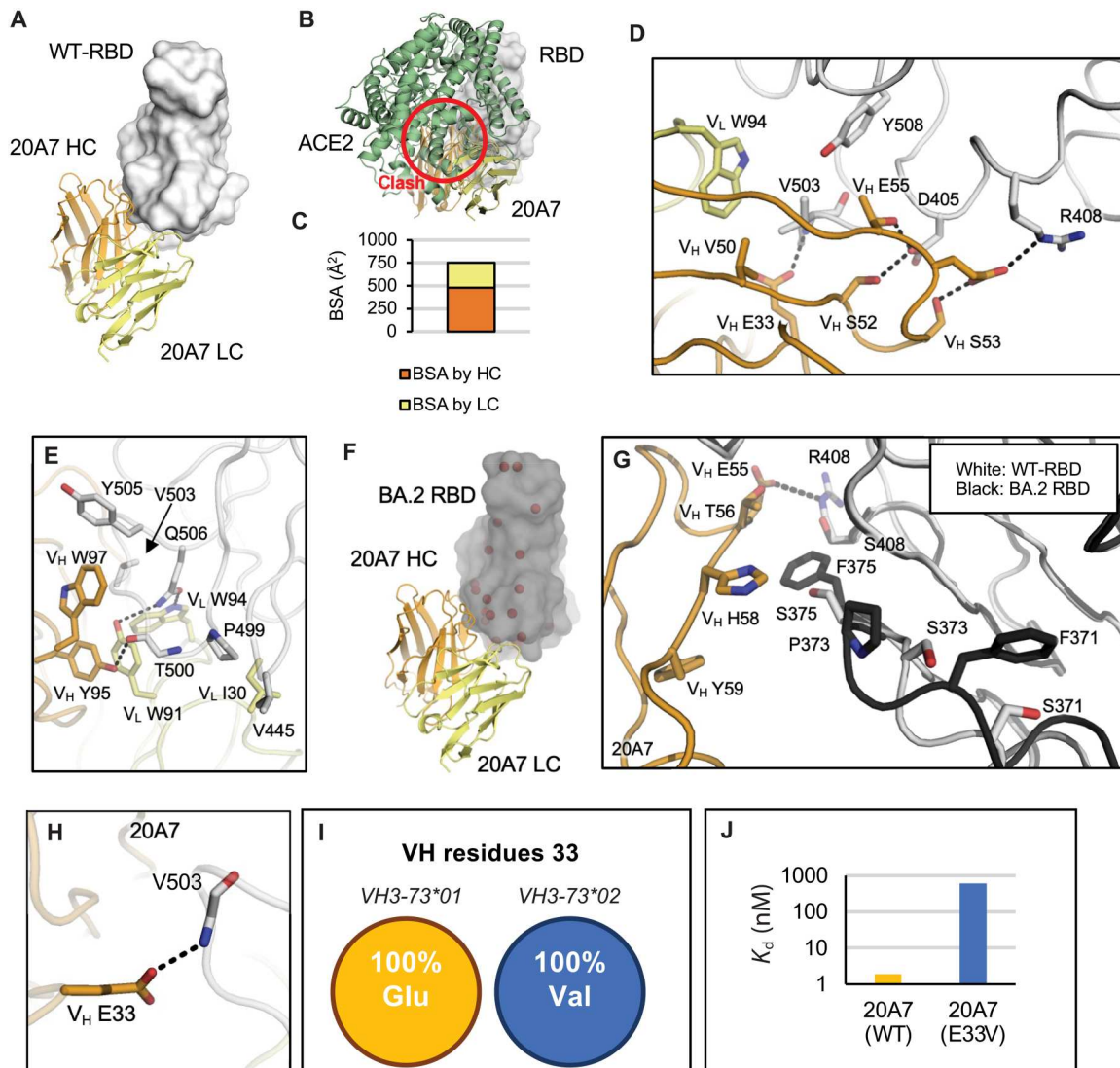
Fig. 4. 20A7 accommodates mutations of SARS-CoV-2 variants. The SARS-CoV-2 wild-type and BA.2 RBDs are shown in white and gray/black, respectively; the heavy and light chains of 20A7 are in orange and yellow, respectively. Hydrogen bonds and salt bridges are indicated by dashed lines. (**A**) The crystal structure of 20A7 in complex with the SARS-CoV-2 wild-type RBD. (**B**) The SARS-CoV-2 RBD in complex with 20A7 superimposed onto an RBD-ACE2 complex structure (PDB 6M0J) shows that 20A7 clashes (red circle) with ACE2. (**C**) The surface area of the SARS-CoV-2 wild-type RBD that is buried by heavy and light chains of 20A7. (**D**) Molecular interactions between the wild-type SARS-CoV-2 RBD and 21B6 CDR H2. (**E**) Molecular interactions between the wild-type SARS-CoV-2 RBD and 21B6 CDR H3. (**F**) The crystal structure of 20A7 with the RBD (BA.2) shows that 20A7 targets BA.2 in the same binding mode as wild-type SARS-CoV-2. Mutated residues in the Omicron BA.2 subvariant are indicated by red spheres. (**G**) Structural comparison of the interaction of 20A7 with wild-type (white) and BA.2 (black) RBDs. (**H**) 20A7 V_H E33 forms a hydrogen bond with the RBD. (**I**) The *VH3-73*01* allele encodes Glu at position 33, whereas *VH3-73*02* encodes Val. (**J**) Biolayer interferometry (BLI) binding assay showed that E33V reduced the binding of 20A7 to the SARS-CoV-2 RBD by about 300-fold.

XBB.1.5 causes a loss of salt bridge with 21B6-V_H D101, which may contribute to some loss of neutralization (Fig. 2G).

20A7 neutralized all SARS-CoV-2 variants tested as well as SARS-CoV (Fig. 2, E and F). The crystal structure of 20A7 with the wild-type SARS-CoV-2 RBD (Fig. 4A) shows that its binding to the RBD would clash with ACE2 (Fig. 4B). Both heavy and light chains interact with the RBD, where the relative RBD surface area buried by heavy and light chains is about 67% and 33%, respectively (Fig. 4C). CDRs H2 (Fig. 4D) and H3 (Fig. 4E) form extensive interactions with the RBD. 20A7 neutralizes Omicron subvariants with little reduction in activity (Fig. 2, E and F). We also determined

a crystal structure of 20A7 in complex with the Omicron BA.2 RBD (Fig. 4F) that exhibited the same binding mode as with the wild-type SARS-CoV-2 RBD (Fig. 4A). Comparison of the interactions of 20A7 with the wild-type and BA.2 variant (Fig. 4G) showed that the salt bridge formed by 20A7 V_H E55 and RBD-R408 was eliminated by the R408S mutation in BA.2, which may contribute to some loss of binding affinity. In addition, mutations at S371, S373, and S375 in the Omicron subvariants induce a localized conformational change in the main chain of a loop containing these residues in the RBD (*26*).

Feng *et al.*, *Sci. Transl. Med.* **15**, eadg7404 (2023)   10 May 2023

7 of 13

Some of the authors of this study previously determined two antibody structures encoded by a highly enriched germline gene, *VH3-73*, in macaques (*27*). In the present study, we show that another *VH3-73*–encoded antibody, 20A7, adopts the same binding mode (fig. S8, A to C). V_H E33 in all three antibodies forms hydrogen bonds with the backbone amide of RBD-V503. V_H E33 is only encoded by the alleles clustered as *VH3-73*01*. In contrast, *VH3-73*02* alleles encode a valine instead of glutamic acid. This single mutation in 20A7, V_H E33V, markedly reduced the binding affinity by about 300-fold, presumably because of the loss of this hydrogen bond (Fig. 4, H to J, and fig. S8), suggesting that it may be difficult to generate such bnAbs in macaques that do not have an *VH3-73*01* allele. We previously made a similar observation that human anti–SARS-CoV-2 *VH2-5/VL2-14* antibodies are also allele specific (*28*). These observations highlight the importance of considering allele polymorphism in vaccine design.

We previously discovered a broad and potent neutralization epitope on the RBDs of SARS-related coronaviruses (*29*). The epitope spans from a corner of RBS-D to the CR3022 site (fig. S9). Here, we show that the broad and potent neutralizing antibodies 25F9 and 20A7 also target this RBS-D/CR3022 site and neutralize all tested SARS-CoV-2 variants as well as other SARS-like viruses. Furthermore, a neutralizing antibody SA55, which is in a clinical trial, potently neutralizes all known SARS-CoV-2 variants, including BQ.1.1 and XBB, and also targets the RBS-D/CR3022 site (fig. S9) (*30*). The features of this site that elicit recurring broad and potent neutralizing antibodies provide a promising target for universal COVID-19 vaccines.

Potent bnAbs show broad sarbecovirus protection in mice

To evaluate the protection conferred by the best bnAbs (25F9 and 20A7) and the best BA.1-neutralizing mAb (27A12), we conducted prophylactic challenge studies in 12-month-old female BALB/c mice with mouse-adapted (MA) sarbecoviruses, including SARS-CoV-2 (MA10), SARS-CoV-2 BA.1, and SARS-CoV (MA15) (*31–33*). We conducted an additional SHC014 challenge study (*34*) for 25F9 because of its extensive neutralization breadth and potency (Fig. 5A). mAbs were administered by intraperitoneal injection at 200 μg per mouse 12 hours before intranasal administration of viruses with 10^3 plaque-forming units (PFU) for SARS-CoV-2 (MA10), 10^4 PFU for SARS-CoV (MA15), and 10^5 PFU for SARS-CoV-2 BA.1 and SHC014 MA15. Mice were monitored for daily weight changes, and lung tissues were collected 2 or 4 days postinfection (dpi) for gross pathology assessment and virus quantification analysis. Mice treated with isotype control antibody exhibited substantial and progressive weight loss due to the infection with all viruses. 25F9 completely prevented weight loss from SARS-CoV-2 (MA10), SARS-CoV (MA15), and SHC014 MA15 infection (Fig. 5B). Although 20A7 and 27A12 showed much higher BA.1 neutralization than 25F9 (IC$_{50}$: 6, 5, and 42 ng/ml, respectively) in vitro (fig. S5C), 25F9 showed the best protection from weight loss after BA.1 infection (Fig. 5B). No signs of lung discoloration (gross pathology) were observed at either 2 or 4 dpi in mice treated with 25F9 (Fig. 5C). Furthermore, we assessed the viral load in the lungs. 25F9 completely abrogated viral replication in all mice at 4 dpi (Fig. 5D). Consistent with in vitro neutralization, 20A7 and 27A12 prophylactic treatment leads to better BA.1 clearance in vivo than 25F9 at 2 dpi (Fig. 5D), suggesting that 25F9 potentially used multi-function for disease protection. We concluded that all three mAbs effectively protected against SARS-CoV-2 (MA10) infection in mice. 25F9 protected against the SARS-CoV-2 BA.1 and other sarbecoviruses equally effectively because it protected against SARS-CoV-2 (MA10), highlighting its potential as a broad and potent sarbecovirus prophylactic antibody.

DISCUSSION

MBCs mature over time after SARS-CoV-2 infection or mRNA vaccination (*34–39*). We recently showed that an AS03, a squalene oil-in-water emulsion adjuvant developed by GlaxoSmithKline, -adjuvanted nanoparticle vaccine conferred durable and heterotypic protection against Omicron challenge with 100% and about 65% protection at 6 weeks and 6 months after the booster, respectively (*11*). The rapid elicitation of bnAbs in serum after the booster suggested the evolution of a broad and potent antibody repertoire encoded in the MBC compartment. Consistent with this notion, we found in this study that SHMs and the potency and breadth of antibodies encoded by B cell receptors in MBCs evolved after the primary vaccination. Those matured MBCs with greater potency and breadth can rapidly differentiate into antibody-secreting cells in response to a booster immunization or infection. Although it is well known that adjuvants can modulate and enhance the magnitude, breadth, and durability of the vaccine-induced serum antibody response, few studies have investigated their effects on the monoclonal level (*28, 40–46*). In this study, we found that the primary vaccination of the AS03-adjuvanted nanoparticle–based subunit vaccine elicited a progressive antibody evolution toward greater potency and breadth over a period of 1 year, presumably driven by antigen-antibody complexes on follicular dendritic cells.

Because of the scarcity of effective mAbs against the Omicron variants (*7, 8, 47–49*) and the potential for zoonotic coronaviruses such as SARS-CoV and MERS-CoV, as well as bat coronaviruses like WIV-1, RaTG13, and SHC014 (*2, 3, 33, 50–54*), to spill over into humans, considerable effort is focused on identifying bnAbs able to cross-neutralize various SARS-CoV-2 variants and other SARS-related viruses. However, there is always a compromise between potency and breadth (*17, 19, 47, 55–57*). Here, we identified seven bnAbs showing potent neutralization against the authentic SARS-CoV-2 WA1 strain with IC$_{50}$ values below 10 ng/ml. All seven mAbs neutralized previous SARS-CoV-2 variants of concern without any reduction in potency. 25F9, 20A7, 21B6, and 27A12 neutralized authentic SARS-CoV-2 BA.1 with IC$_{50}$ values of 42, 6, 11, and 5 ng/ml, respectively. 27A12 showed little, if any, reduction in neutralization against SARS-CoV-2 BA.2, BA.3, BA.4/5, BQ.1, BQ.1.1, and XBB relative to BA.1. 25F9 and 20A7 neutralized authentic SARS-CoV and several other bat coronaviruses with comparable potency as compared to that against SARS-CoV-2, although 20A7 showed some reduction of neutralization against a Pangolin strain. Furthermore, we determined crystal structures of mAbs (25F9, 20A7, and 21B6) and their mode of binding to the RBD of SARS-CoV-2, as well as one structure of 21B6 complexed with the RBD of SARS-CoV-2 BA.2, at resolutions of 3.05, 2.58, 1.75, and 2.30 Å, respectively. Despite targeting the same overall region in the RBD, namely, "RBS-D/CR3022" (fig. S10) (*28*), antibodies such as ADG20, DH1047, and S2X259 (*29, 47*) lost neutralization potency against Omicron and its subvariants. In contrast, other antibodies such as 20A7, identified in this study, and SA55 are largely resistant to mutations observed in the Omicron subvariants.
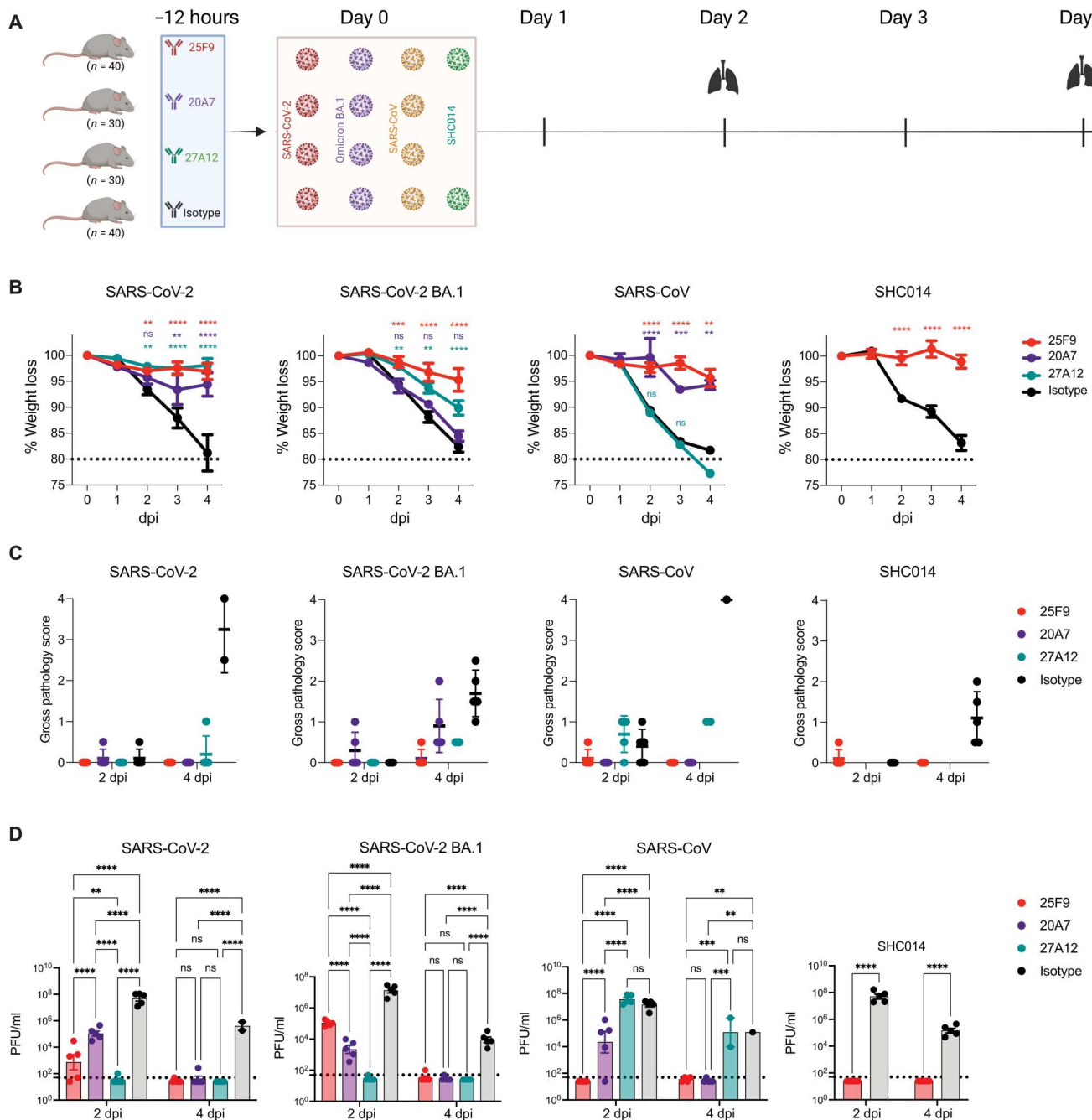
Fig. 5. 25F9, 20A7, and 27A12 protect aged mice from SARS-CoV-2 and other sarbecovirus-induced pathology. (**A**) A diagram depicting the challenge study in mice. 25F9, 20A7, 27A12, or a DENV2(2D22) control antibody were administered intraperitoneally at 200 μg per animal into 14 groups of aged mice (10 animals per group). Animals were challenged intranasally 12 hours after antibody infusion with one of the indicated sarbecoviruses (mouse-adapted SARS-CoV-2, 1×10^3 PFU; mouse-adapted SARS-CoV-2-BA.1, 1×10^5 PFU; mouse-adapted SARS-CoV, 1×10^4 PFU; or SHC014 MA15, 1×10^5 PFU). Lungs were collected on day 2 or 4 after infection. As a control, groups of mice were exposed only to phosphate-buffered saline in the absence of virus. (**B**) The body weight change of mice after challenge with mouse-adapted SARS-CoV-2, SARS-CoV-2 BA.1, SARS-CoV, and SHC014, respectively. Data are presented as means ± SEM from 10 animals per group from days 0 to 2 or 5 animals per group from days 3 to 4. Data were analyzed using a mixed-effects model with post hoc Dunnett's multiple tests in comparison with the control group; significance is indicated as **P < 0.01, ***P < 0.001, and ****P < 0.0001 or ns when not significant. The dotted horizontal line at 80% designates a weight loss amount at which softened mouse food was added to the cages. (**C**) Lung gross pathology was scored at the collection on days 2 and 4 after infection in mice prophylactically treated with indicated bnAbs or the isotype control mAb (*n* = 5 per group). Individual mice are represented by the dot plots. Data are presented as means ± SEM. (**D**) Lung virus titers (PFU per lung) were determined by plaque assay of lung tissues collected at day 2 or 4 after infection (*n* = 5 individuals per time point for each group). Data are shown as scatter dot plots with bar heights representing the mean and whiskers representing SEM. Data were analyzed with a mixed-effects model with post hoc Dunnett's multiple tests in comparison with the control group; significance is indicated as **P < 0.01, ***P < 0.001, and ****P < 0.0001 or ns when not significant. The dotted horizontal line indicates the limit of detection (50 PFU) for the plaque assay. For samples with values below this, data are plotted at half the limit of detection.

Multiple factors can affect resistance or loss of neutralization potency of antibodies, including but not limited to decreases in binding affinity, angles of approach to an epitope, and dependence on particular residues in the epitope that might affect the binding of one antibody and not another. Nevertheless, as we and others have shown, this region in the RBD has the potential to elicit broad and potent antibodies. Thus, molecular understanding of how different antibodies are able to target this region can provide valuable insights for epitope-focused, next-generation vaccine design.

Last, 25F9, 20A7, and 27A12 were evaluated for their prophylactic protection efficacy against four different SARS-related viruses, including mouse-adapted SARS-CoV-2 MA10, SARS-CoV-2 BA.1, SARS-CoV MA15, and SHC014 MA15 in aged mice. This mouse model is well recognized for its efficient recapitulation of disease pathogenesis (58). Our results demonstrated that prophylactic treatment with a single dose of bnAbs led not only to clinical improvement, as shown by the absence of weight loss, but also to markedly reduced lung pathology, virus load, and inflammatory infiltration. Rhesus macaque–derived antibodies have some potential issues of immunogenicity in humans. However, animal-derived antibodies have been widely used in clinical trials, such as mouse-derived humanized antibodies, trastuzumab, bevacizumab, and natalizumab (59). Furthermore, nonhuman primates are the closest living relatives of human beings, and rhesus macaque–derived mAbs could have better performance than mouse-derived mAbs in clinical use.

Our study has some limitations. A direct longitudinal comparison between a nonadjuvanted and adjuvanted group of vaccinees could not be made because of the unavailability of blood samples. Whether the same degree of antibody maturation and bnAbs will be observed without an adjuvant or with other adjuvants, or in humans, needs further investigation. In addition, it will be vitally important to identify antibody escape mutants and evaluate the emergence in vivo of pathogenic variants in the presence of antibody. The focus of the current study is the isolation and extensive characterization of MBC-derived mAbs that demonstrate potent and broad neutralization capacity despite a lack of such neutralization activity in serum, as shown in the summary of our study (fig. S11). In conclusion, we identified 25F9 and 20A7 as two highly potent bnAbs, making them promising prophylactic candidates against sarbecovirus infection.

MATERIALS AND METHODS
Study design
The study used banked blood samples from our previous study (10, 11), in which two groups of male rhesus macaques (*M. Mulatta*) were involved. The first group of five animals received two doses of RBD-NP (RBD protein from the ancestral strain displayed on I53-50 nanoparticles), and the second group, comprising six animals, received two doses of HexaPro-NP (HexaPro spike protein from the ancestral strain displayed on I53-50 nanoparticles). Both immunogens were administered with the AS03 adjuvant on days 0 and 21 using a prime-boost regimen. All 11 animals from both groups were boosted with an I53-50 nanoparticle immunogen displaying the RBD from the beta variant about a year after the first immunization series. The number of animals in each group was determined to identify large differences between groups on the basis of our previous experience. We did not do a power calculation to determine the sample size. The animals were randomly distributed between groups, considering body weight and age as the critical variables. The investigators were not blinded to allocation during experiments and outcome assessment.

Statistical analysis
Individual-level data for all the figures are presented in data file S1. The difference between any two groups at a time point was measured using a two-tailed nonparametric Mann-Whitney unpaired rank sum test or the two-tailed Kruskal-Wallis test with subsequent Dunn's multiple-comparisons test. The difference between groups at different time points was measured using two-way analysis of variance (ANOVA). The difference between multiple time points was measured using one-way ANOVA. The difference between different categories was measured by the two-tailed chi-square test. All correlations were Spearman's correlations based on ranks. All statistical analyses were performed using GraphPad Prism v.9.0.0 or R version 3.6.1. All the figures were made in GraphPad Prism or R and organized in Adobe Illustrator. Cartoons were created with BioRender.com.

Supplementary Materials
This PDF file includes:
Materials and Methods
Figs. S1 to S11
Tables S1 to S3
References (60–73)

Other Supplementary Material for this manuscript includes the following:
Data file S1
MDAR Reproducibility Checklist

View/request a protocol for this paper from *Bio-protocol*.

REFERENCES AND NOTES
1. J. S. M. Peiris, K. Y. Yuen, A. D. M. E. Osterhaus, K. Stohr, The severe acute respiratory syndrome. *N. Engl. J. Med.* **349**, 2431–2441 (2003).
2. P. Zhou, X.-L. Yang, X.-G. Wang, B. Hu, L. Zhang, W. Zhang, H.-R. Si, Y. Zhu, B. Li, C.-L. Huang, H.-D. Chen, J. Chen, Y. Luo, H. Guo, R.-D. Jiang, M.-Q. Liu, Y. Chen, X.-R. Shen, X. Wang, X.-S. Zheng, K. Zhao, Q.-J. Chen, F. Deng, L.-L. Liu, B. Yan, F.-X. Zhan, Y.-Y. Wang, G.-F. Xiao, Z.-L. Shi, Addendum: A pneumonia outbreak associated with a new coronavirus of probable bat origin. *Nature* **588**, E6 (2020).
3. A. M. Zaki, S. van Boheemen, T. M. Bestebroer, A. D. M. E. Osterhaus, R. A. M. Fouchier, Isolation of a novel coronavirus from a man with pneumonia in Saudi Arabia. *N. Engl. J. Med.* **367**, 1814–1820 (2012).
4. S. Collie, J. Nayager, L. Bamford, L. G. Bekker, M. Zylstra, G. Gray, Effectiveness and durability of the BNT162b2 vaccine against omicron sublineages in South Africa. *N. Engl. J. Med.* **387**, 1332–1333 (2022).
5. G. Regev-Yochay, T. Gonen, M. Gilboa, M. Mandelboim, V. Indenbaum, S. Amit, L. Meltzer, K. Asraf, C. Cohen, R. Fluss, A. Biber, I. Nemet, L. Kliker, G. Joseph, R. Doolman, E. Mendelson, L. S. S. Freedman, D. Harats, Y. Kreiss, Y. Lustig, Efficacy of a fourth dose of Covid-19 mRNA vaccine against omicron. *N. Engl. J. Med.* **386**, 1377–1380 (2022).
6. H. F. Tseng, B. K. Ackerson, K. J. Bruxvoort, L. S. Sy, J. E. Tubert, G. S. Lee, J. H. Ku, A. Florea, Y. Luo, S. Qiu, S. K. Choi, H. S. Takhar, M. Aragones, Y. D. Paila, S. Chavers, C. A. Talarico, L. Qian, Effectiveness of mRNA-1273 vaccination against SARS-CoV-2 omicron subvariants BA.1, BA.2, BA.2.12.1, BA.4, and BA.5. *Nat. Commun.* **14**, 189 (2023).
7. E. Takashita, S. Yamayoshi, V. Simon, H. van Bakel, E. M. Sordillo, A. Pekosz, S. Fukushi, T. Suzuki, K. Maeda, P. Halfmann, Y. Sakai-Tagawa, M. Ito, S. Watanabe, M. Imai, H. Hasegawa, Y. Kawaoka, Efficacy of antibodies and antiviral drugs against omicron BA.2.12.1, BA.4, and BA.5 subvariants. *N. Engl. J. Med.* **387**, 468–470 (2022).
8. Q. Wang, S. Iketani, Z. Li, L. Liu, Y. Guo, Y. Huang, A. D. Bowen, M. Liu, M. Wang, J. Yu, R. Valdez, A. S. Lauring, Z. Sheng, H. H. Wang, A. Gordon, L. Liu, D. D. Ho, Alarming antibody

evasion properties of rising SARS-CoV-2 BQ and XBB subvariants. *Cell* **186**, 279–286.e8 (2022).

9. A. A. Cohen, N. van Doremalen, A. J. Greaney, H. Andersen, A. Sharma, T. N. Starr, J. R. Keeffe, C. Fan, J. E. Schulz, P. N. P. Gnanapragasam, L. M. Kakutani, A. P. WestJr, G. Saturday, Y. E. Lee, H. Gao, C. A. Jette, M. G. Lewis, T. K. Tan, A. R. Townsend, J. D. Bloom, V. J. Munster, P. J. Bjorkman, Mosaic RBD nanoparticles protect against challenge by diverse sarbecoviruses in animal models. *Science* **377**, eabq0839 (2022).

10. P. S. Arunachalam, A. C. Walls, N. Golden, C. Atyeo, S. Fischinger, C. F. Li, P. Aye, M. J. Navarro, L. L. Lai, V. V. Edara, K. Roltgen, K. Rogers, L. Shirreff, D. E. Ferrell, S. Wrenn, D. Pettie, J. C. Kraft, M. C. Miranda, E. Kepl, C. Sydeman, N. Brunette, M. Murphy, B. Fiala, L. Carter, A. G. White, M. Trisal, C. L. Hsieh, K. Russell-Lodrigue, C. Monjure, J. Dufour, S. Spencer, L. Doyle-Meyers, R. P. Bohm, N. J. Maness, C. Roy, J. A. Plante, K. S. Plante, A. Zhu, M. J. Gorman, S. Shin, X. Y. Shen, J. Fontenot, S. Gupta, D. T. O'Hagan, R. Van Der Most, R. Rappuoli, R. L. Coffman, D. Novack, J. S. McLellan, S. Subramaniam, D. Montefiori, S. D. Boyd, J. J. Flynn, G. Alter, F. Villinger, H. Kleanthous, J. Rappaport, M. S. Suthar, N. P. King, D. Veesler, B. Pulendran, Adjuvanting a subunit COVID-19 vaccine to induce protective immunity. *Nature* **594**, 253–258 (2021).

11. P. S. Arunachalam, Y. P. Feng, U. Ashraf, M. Y. Hu, A. C. Walls, V. V. Edara, V. I. Zarnitsyna, P. P. Aye, N. Golden, M. C. Miranda, K. W. M. Green, B. M. Threeton, N. J. Maness, B. J. Beddingfield, R. P. Bohm, S. E. Scheuermann, K. Goff, J. Dufour, K. Russell-Lodrigue, E. Kepl, B. Fiala, S. Wrenn, R. Ravichandran, D. Ellis, L. Carter, K. Rogers, L. M. Shirreff, D. E. Ferrell, N. R. D. Adhikary, J. Fontenot, H. L. Hammond, M. Frieman, A. Grifoni, A. Sette, D. T. O'Hagan, R. Van der Most, R. Rappuoli, F. Villinger, H. Kleanthous, J. Rappaport, M. S. Suthar, D. Veesler, T. T. Wang, N. P. King, B. Pulendran, Durable protection against the SARS-CoV-2 Omicron variant is induced by an adjuvanted subunit vaccine. *Sci. Transl. Med.* **14**, eabq4130 (2022).

12. A. C. Walls, M. C. Miranda, A. Schafer, M. N. Pham, A. Greaney, P. S. Arunachalam, M. J. Navarro, M. A. Tortorici, K. Rogers, M. A. O'Connor, L. Shirreff, D. E. Ferrell, J. Bowen, N. Brunette, E. Kepl, S. K. Zepeda, T. Starr, C. L. Hsieh, B. Fiala, S. Wrenn, D. Pettie, C. Sydeman, K. R. Sprouse, M. Johnson, A. Blackstone, R. Ravichandran, C. Ogohara, L. Carter, S. W. Tilles, R. Rappuoli, S. R. Leist, D. R. Martinez, M. Clark, R. Tisch, D. T. O'Hagan, R. Van der Most, W. C. Van Voorhis, D. Corti, J. S. McLellan, H. Kleanthous, T. P. Sheahan, K. D. Smith, D. H. Fuller, F. Villinger, J. Bloom, B. Pulendran, R. S. Baric, N. P. King, D. Veesler, Elicitation of broadly protective sarbecovirus immunity by receptor-binding domain nanoparticle vaccines. *Cell* **184**, 5432–5447.e16 (2021).

13. X. Brochet, M. P. Lefranc, V. Giudicelli, IMGT/V-QUEST: The highly customized and integrated system for IG and TR standardized V-J and V-D-J sequence analysis. *Nucleic Acids Res.* **36**, W503–W508 (2008).

14. N. Vazquez Bernat, M. Corcoran, I. Nowak, M. Kaduk, X. Castro Dopico, S. Narang, P. Maisonasse, N. Dereuddre-Bosquet, B. Murrell, G. B. Karlsson Hedestam, Rhesus and cynomolgus macaque immunoglobulin heavy-chain genotyping yields comprehensive databases of germline VDJ alleles. *Immunity* **54**, 355–366.e4 (2021).

15. M. Yuan, H. Liu, N. Wu, C. Lee, X. Zhu, F. Zhao, D. Huang, W. Yu, Y. Hua, H. Tien, T. Rogers, E. Landais, D. Sok, J. Jardine, D. Burton, I. Wilson, Structural basis of a shared antibody response to SARS-CoV-2. *Science* **369**, 1119–1123 (2020).

16. E. Andreano, I. Paciello, G. Piccini, N. Manganaro, P. Pileri, I. Hyseni, M. Leonardi, E. Pantano, V. Abbiento, L. Benincasa, G. Giglioli, C. De Santi, M. Fabbiani, I. Rancan, M. Tumbarello, F. Montagnani, C. Sala, E. Montomoli, R. Rappuoli, Hybrid immunity improves B cells and antibodies against SARS-CoV-2 variants. *Nature* **600**, 530–535 (2021).

17. Z. J. Wang, F. Schmidt, Y. Weisblum, F. Muecksch, C. O. Barnes, S. Finkin, D. Schaefer-Babajew, M. Cipolla, C. Gaebler, J. A. Lieberman, T. Y. Oliveira, Z. Yang, M. E. Abernathy, K. E. Huey-Tubman, A. Hurley, M. Turroja, K. A. West, K. Gordon, K. G. Millard, V. Ramos, J. Da Silva, J. L. Xu, R. A. Colbert, R. Patel, J. Dizon, C. Unson-O'Brien, I. Shimeliovich, A. Gazumyan, M. Caskey, P. J. Bjorkman, R. Casellas, T. Hatziioannou, P. D. Bieniasz, M. C. Nussenzweig, mRNA vaccine-elicited antibodies to SARS-CoV-2 and circulating variants. *Nature* **592**, 616–622 (2021).

18. T. Starr, N. Czudnochowski, Z. Liu, F. Zatta, Y. Park, A. Addetia, D. Pinto, M. Beltramello, P. Hernandez, A. Greaney, R. Marzi, W. Glass, I. Zhang, A. Dingens, J. Bowen, M. Tortorici, A. Walls, J. Wojcechowskyj, A. De Marco, L. Rosen, J. Zhou, M. Montiel-Ruiz, H. Kaiser, J. Dillen, H. Tucker, J. Bassi, C. Silacci-Fregni, M. Housley, J. di Iulio, G. Lombardo, M. Agostini, N. Sprugasci, K. Culap, S. Jaconi, A. Meury, E. Dellota, R. Abdelnabi, S. Foo, E. Cameroni, S. Stumpf, T. Croll, J. Nix, C. Havenar-Daughton, L. Piccoli, F. Benigni, J. Neyts, A. Telenti, F. Lempp, M. Pizzuto, J. Chodera, C. Hebner, H. Virgin, S. Whelan, D. Veesler, D. Corti, J. Bloom, G. Snell, SARS-CoV-2 RBD antibodies that maximize breadth and resistance to escape. *Nature* **597**, 97–102 (2021).

19. C. G. Rappazzo, L. V. Tse, C. I. Kaku, D. Wrapp, M. Sakharkar, D. L. Huang, L. M. Deveau, T. J. Yockachonis, A. S. Herbert, M. B. Battles, C. M. O'Brien, M. E. Brown, J. C. Geoghegan, J. Belk, L. H. Peng, L. L. Yang, Y. X. Hou, T. D. Scobey, D. R. Burton, D. Nemazee, J. M. Dye, J. E. Voss, B. M. Gunn, J. S. McLellan, R. S. Baric, L. E. Gralinski, L. M. Walker, Broad and potent

activity against SARS-like viruses by an engineered human monoclonal antibody. *Science* **371**, 823–829 (2021).

20. T. N. Starr, S. K. Zepeda, A. C. Walls, A. J. Greaney, S. Alkhovsky, D. Veesler, J. D. Bloom, ACE2 binding is an ancestral and evolvable trait of sarbecoviruses. *Nature* **603**, 913–918 (2022).

21. M. Yuan, N. Wu, X. Zhu, C. Lee, R. So, H. Lv, C. Mok, I. Wilson, A highly conserved cryptic epitope in the receptor binding domains of SARS-CoV-2 and SARS-CoV. *Science* **368**, 630–633 (2020).

22. J. Kreye, S. Reincke, H. Kornau, E. Sanchez-Sendin, V. Corman, H. Liu, M. Yuan, N. Wu, X. Zhu, C. Lee, J. Trimpert, M. Holtje, K. Dietert, L. Stoffler, N. von Wardenburg, S. van Hoof, M. Homeyer, J. Hoffmann, A. Abdelgawad, A. Gruber, L. Bertzbach, D. Vladimirova, L. Li, P. Barthel, K. Skriner, A. Hocke, S. Hippenstiel, M. Witzenrath, N. Suttorp, F. Kurth, C. Franke, M. Endres, D. Schmitz, L. Jeworowski, A. Richter, M. Schmidt, T. Schwarz, M. Muller, C. Drosten, D. Wendisch, L. Sander, N. Osterrieder, I. Wilson, H. Pruss, A therapeutic non-self-reactive SARS-CoV-2 antibody protects from Lung Pathology in a COVID-19 hamster model. *Cell* **183**, 1058–1069.e19 (2020).

23. M. Tortorici, N. Czudnochowski, T. Starr, R. Marzi, A. Walls, F. Zatta, J. Bowen, S. Jaconi, J. Di Iulio, Z. Wang, A. De Marco, S. Zepeda, D. Pinto, Z. Liu, M. Beltramello, I. Bartha, M. Housley, F. Lempp, L. Rosen, E. Dellota, H. Kaiser, M. Montiel-Ruiz, J. Zhou, A. Addetia, B. Guarino, K. Culap, N. Sprugasci, C. Saliba, E. Vetti, I. Giacchetto-Sasselli, C. Fregni, R. Abdelnabi, S. Foo, C. Havenar-Daughton, M. Schmid, F. Benigni, E. Cameroni, J. Neyts, A. Telenti, H. Virgin, S. Whelan, G. Snell, J. Bloom, D. Corti, D. Veesler, M. Pizzuto, Broad sarbecovirus neutralization by a human monoclonal antibody. *Nature* **597**, 103–108 (2021).

24. M. Tortorici, M. Beltramello, F. Lempp, D. Pinto, H. Dang, L. Rosen, M. McCallum, J. Bowen, A. Minola, S. Jaconi, F. Zatta, A. De Marco, B. Guarino, S. Bianchi, E. Lauron, H. Tucker, J. Zhou, A. Peter, C. Havenar-Daughton, J. Wojcechowskyj, J. Case, R. Chen, H. Kaiser, M. Montiel-Ruiz, M. Meury, N. Czudnochowski, R. Spreafico, J. Dillen, C. Ng, N. Sprugasci, K. Culap, F. Benigni, R. Abdelnabi, S. Foo, M. Schmid, E. Cameroni, A. Riva, A. Gabrieli, M. Galli, M. Pizzuto, J. Neyts, M. Diamond, H. Virgin, G. Snell, D. Corti, K. Fink, D. Veesler, Ultrapotent human antibodies protect against SARS-CoV-2 challenge via multiple mechanisms. *Science* **370**, 950–957 (2020).

25. D. Pinto, Y.-J. Park, M. Beltramello, A. C. Walls, M. A. Tortorici, S. Bianchi, S. Jaconi, K. Culap, F. Zatta, A. D. Marco, A. Peter, B. Guarino, R. Spreafico, E. Cameroni, J. B. Case, R. E. Chen, C. Havenar-Daughton, G. Snell, A. Telenti, H. W. Virgin, A. Lanzavecchia, M. S. Diamond, K. Fink, D. Veesler, D. Corti, Cross-neutralization of SARS-CoV-2 by a human monoclonal SARS-CoV antibody. *Nature* **583**, 290–295 (2020).

26. Y.-J. Park, D. Pinto, A. C. Walls, Z. Liu, A. D. Marco, F. Benigni, F. Zatta, C. Silacci-Fregni, J. Bassi, K. R. Sprouse, A. Addetia, J. E. Bowen, C. Stewart, M. Giurdanella, C. Saliba, B. Guarino, M. A. Schmid, N. M. Franko, J. K. Logue, H. V. Dang, K. Hauser, J. di Iulio, W. Rivera, G. Schnell, A. Rajesh, J. Zhou, N. Farhat, H. Kaiser, M. Montiel-Ruiz, J. Noack, F. A. Lempp, J. Janer, R. Abdelnabi, P. Maes, P. Ferrari, A. Ceschi, O. Giannini, G. D. de Melo, L. Kergoat, H. Bourhy, J. Neyts, L. Soriaga, L. A. Purcell, G. Snell, S. P. J. Whelan, A. Lanzavecchia, H. W. Virgin, L. Piccoli, H. Y. Chu, M. S. Pizzuto, D. Corti, D. Veesler, Imprinted antibody responses against SARS-CoV-2 Omicron sublineages. *Science* **378**, 619–627 (2022).

27. W. He, M. Yuan, S. Callaghan, R. Musharrafieh, G. Song, M. Silva, N. Beutler, W. H. Lee, P. Yong, J. L. Torres, M. Melo, P. P. Zhou, F. Z. Zhao, X. Y. Zhu, L. H. Peng, D. L. Huang, F. Anzanello, J. Ricketts, M. Parren, E. Garcia, M. Ferguson, W. Rinaldi, S. A. Rawlings, D. Nemazee, D. M. Smith, B. Briney, Y. Safonova, T. F. Rogers, J. M. Dan, Z. L. Zhang, D. Weiskopf, A. Sette, S. Crotty, D. J. Irvine, A. B. Ward, I. A. Wilson, D. R. Burton, R. Andrabi, Broadly neutralizing antibodies to SARS-related viruses can be readily induced in rhesus macaques. *Sci. Transl. Med.* **14**, eabl9605 (2022).

28. M. Yuan, Y. Wang, H. Lv, T. J. C. Tan, I. A. Wilson, N. C. Wu, Molecular analysis of a public cross-neutralizing antibody response to SARS-CoV-2. *Cell Rep.* **41**, 111650 (2022).

29. M. Yuan, X. Zhu, W. T. He, P. Zhou, C. I. Kaku, T. Capozzola, C. Y. Zhu, X. Yu, H. Liu, W. Yu, Y. Hua, H. Tien, L. Peng, G. Song, C. A. Cottrell, W. R. Schief, D. Nemazee, L. M. Walker, R. Andrabi, D. R. Burton, I. A. Wilson, A broad and potent neutralization epitope in SARS-related coronaviruses. *Proc. Natl. Acad. Sci. U.S.A.* **119**, e2205784119 (2022).

30. Y. Cao, F. Jian, J. Wang, Y. Yu, W. Song, A. Yisimayi, J. Wang, R. An, X. Chen, N. Zhang, Y. Wang, P. Wang, L. Zhao, H. Sun, L. Yu, S. Yang, X. Niu, T. Xiao, Q. Gu, F. Shao, X. Hao, Y. Xu, R. Jin, Z. Shen, Y. Wang, X. S. Xie, Imprinted SARS-CoV-2 humoral immunity induces convergent Omicron RBD evolution. *Nature* **614**, 521–529 (2023).

31. A. Roberts, D. Deming, C. D. Paddock, A. Cheng, B. Yount, L. Vogel, B. D. Herman, T. Sheahan, M. Heise, G. L. Genrich, S. R. Zaki, R. Baric, K. Subbarao, A mouse-adapted SARS-coronavirus causes disease and mortality in BALB/c mice. *PLOS Pathog.* **3**, e5 (2007).

32. S. R. Leist, K. H. Dinnon 3rd, A. Schafer, L. V. Tse, K. Okuda, Y. J. Hou, A. West, C. E. Edwards, W. Sanders, E. J. Fritch, K. L. Gully, T. Scobey, A. J. Brown, T. P. Sheahan, N. J. Moorman, R. C. Boucher, L. E. Gralinski, S. A. Montgomery, R. S. Baric, A mouse-adapted SARS-CoV-2 induces acute lung injury and mortality in standard laboratory mice. *Cell* **183**, 1070–1085.e12 (2020).

33. V. D. Menachery, B. L. Yount, K. Debbink, S. Agnihothram, L. E. Gralinski, J. A. Plante, R. L. Graham, T. Scobey, X. Y. Ge, E. F. Donaldson, S. H. Randell, A. Lanzavecchia,

Feng *et al.*, *Sci. Transl. Med.* **15**, eadg7404 (2023)   10 May 2023

11 of 13

W. A. Marasco, Z. L. L. Shi, R. S. Baric, A SARS-like cluster of circulating bat coronaviruses shows potential for human emergence. *Nat. Med.* **21**, 1508–1513 (2015).

34. D. R. Martinez, A. Schafer, S. R. Leist, G. De la Cruz, A. West, E. N. Atochina-Vasserman, L. C. Lindesmith, N. Pardi, R. Parks, M. Barr, D. Li, B. Yount, K. O. Saunders, D. Weissman, B. F. Haynes, S. A. Montgomery, R. S. Baric, Chimeric spike mRNA vaccines protect against Sarbecovirus challenge in mice. *Science* **373**, 991–998 (2021).

35. C. Gaebler, Z. Wang, J. Lorenzi, F. Muecksch, S. Finkin, M. Tokuyama, A. Cho, M. Jankovic, D. Schaefer-Babajew, T. Oliveira, M. Cipolla, C. Viant, C. Barnes, Y. Bram, G. Breton, T. Hagglof, P. Mendoza, A. Hurley, M. Turroja, K. Gordon, K. Millard, V. Ramos, F. Schmidt, Y. Weisblum, D. Jha, M. Tankelevich, G. Martinez-Delgado, J. Yee, R. Patel, J. Dizon, C. Unson-O'Brien, I. Shimeliovich, D. Robbiani, Z. Zhao, A. Gazumyan, R. Schwartz, T. Hatziioannou, P. Bjorkman, S. Mehandru, P. Bieniasz, M. Caskey, M. Nussenzweig, Evolution of antibody immunity to SARS-CoV-2. *Nature* **591**, 639–644 (2021).

36. M. Sakharkar, C. Rappazzo, W. Wieland-Alter, C. Hsieh, D. Wrapp, E. Esterman, C. Kaku, A. Wec, J. Geoghegan, J. McLellan, R. Connor, P. Wright, L. Walker, Prolonged evolution of the human B cell response to SARS-CoV-2 infection. *Sci. Immunol.* **6**, eabg6916 (2021).

37. A. Sokal, P. Chappert, G. Barba-Spaeth, A. Roeser, S. Fourati, I. Azzaoui, A. Vandenberghe, I. Fernandez, A. Meola, M. Bouvier-Alias, E. Crickx, A. Beldi-Ferchiou, S. Hue, L. Languille, M. Michel, S. Baloul, F. Noizat-Pirenne, M. Luka, J. Megret, M. Menager, J. Pawlotsky, S. Fillatreau, F. Rey, J. Weill, C. Reynaud, M. Mahevas, Maturation and persistence of the anti-SARS-CoV-2 memory B cell response. *Cell* **184**, 1201–1213.e14 (2021).

38. F. Muecksch, Y. Weisblum, C. O. Barnes, F. Schmidt, D. Schaefer-Babajew, Z. J. Wang, J. C. C. Lorenzi, A. I. Flyak, A. T. DeLaitsch, K. E. Huey-Tubman, S. R. Hou, C. A. Schiffer, C. Gaebler, J. Da Silva, D. Poston, S. Finkin, A. Cho, M. Cipolla, T. Y. Oliveira, K. G. Millard, V. Ramos, A. Gazumyan, M. Rutkowska, M. Caskey, M. C. Nussenzweig, P. J. Bjorkman, T. Hatziioannou, P. D. Bieniasz, Affinity maturation of SARS-CoV-2 neutralizing antibodies confers potency, breadth, and resilience to viral escape mutations. *Immunity* **54**, 1853–1868.e7 (2021).

39. W. Kim, J. Q. Zhou, S. C. Horvath, A. J. Schmitz, A. J. Sturtz, T. Lei, Z. Liu, E. Kalaidina, M. Thapa, W. B. Alsoussi, A. Haile, M. K. Klebert, T. Suessen, L. Parra-Rodriguez, P. A. Mudd, S. P. J. Whelan, W. D. Middleton, S. A. Teefey, I. Pusic, J. A. O'Halloran, R. M. Presti, J. S. Turner, A. H. Ellebedy, Germinal centre-driven maturation of B cell response to mRNA vaccination. *Nature* **604**, 141–145 (2022).

40. B. Pulendran, P. S. Arunachalam, D. T. O'Hagan, Emerging concepts in the science of vaccine adjuvants. *Nat. Rev. Drug Discov.* **20**, 454–475 (2021).

41. A. H. Ellebedy, R. Nachbagauer, K. J. L. Jackson, Y. N. Dai, J. Han, W. B. Alsoussi, C. W. Davis, D. Stadlbauer, N. Rouphael, V. Chromikova, M. McCausland, C. Y. Chang, M. Cortese, M. Bower, C. Chennareddy, A. J. Schmitz, V. I. Zarnitsyna, L. L. Lai, A. Rajabhathor, C. Kazemian, R. Antia, M. J. Mulligan, A. B. Ward, D. H. Fremont, S. D. Boyd, B. Pulendran, F. Krammer, R. Ahmed, Adjuvanted H5N1 influenza vaccine enhances both cross-reactive memory B cell and strain-specific naive B cell responses in humans. *Proc. Natl. Acad. Sci. U.S.A.* **117**, 17957–17964 (2020).

42. D. T. O'Hagan, R. van der Most, R. N. Lodaya, M. Coccia, G. Lofano, "World in motion" - emulsion adjuvants rising to meet the pandemic challenges. *NPJ Vaccines* **6**, 158 (2021).

43. S. Khurana, W. Chearwae, F. Castellino, J. Manischewitz, L. R. King, A. Honorkiewicz, M. T. Rock, K. M. Edwards, G. D. Giudice, R. Rappuoli, H. Golding, Vaccines with MF59 adjuvant expand the antibody repertoire to target protective sites of pandemic avian H5N1 influenza virus. *Sci. Transl. Med.* **2**, 15ra5 (2010).

44. S. Khurana, N. Verma, J. W. Yewdell, A. K. Hilbert, F. Castellino, M. Lattanzi, G. D. Giudice, R. Rappuoli, H. Golding, MF59 adjuvant enhances diversity and affinity of antibody-mediated immune response to pandemic influenza vaccines. *Sci. Transl. Med.* **3**, 85ra48 (2011).

45. K. Y. Chung, E. M. Coyle, D. Jani, L. R. King, R. Bhardwaj, L. Fries, G. Smith, G. Glenn, H. Golding, S. Khurana, ISCOMATRIX adjuvant promotes epitope spreading and antibody affinity maturation of influenza A H7N9 virus like particle vaccine that correlate with virus neutralization in humans. *Vaccine* **33**, 3953–3962 (2015).

46. S. Khurana, E. M. Coyle, J. Manischewitz, L. R. King, J. Gao, R. N. Germain, P. L. Schwartzberg, J. S. Tsang, H. Golding, AS03-adjuvanted H5N1 vaccine promotes antibody diversity and affinity maturation, NAI titers, cross-clade H5N1 neutralization, but not H1N1 cross-subtype neutralization. *NPJ Vaccines* **3**, 40 (2018).

47. E. Cameroni, J. E. Bowen, L. E. Rosen, C. Saliba, S. K. Zepeda, K. Culap, D. Pinto, L. A. VanBlargan, A. De Marco, J. di Iulio, F. Zatta, H. Kaiser, J. Noack, N. Farhat, N. Czudnochowski, C. Havenar-Daughton, K. R. Sprouse, J. R. Dillen, A. E. Powell, A. Chen, C. Maher, L. Yin, D. Sun, L. Soriaga, J. Bassi, C. Silacci-Fregni, C. Gustafsson, N. M. Franko, J. Logue, N. T. Iqbal, I. Mazzitelli, J. Geffner, R. Grifantini, H. Chu, A. Gori, A. Riva, O. Giannini, A. Ceschi, P. Ferrari, P. E. Cippa, A. Franzetti-Pellanda, C. Garzoni, P. J. Halfmann, Y. Kawaoka, C. Hebner, L. A. Purcell, L. Piccoli, M. S. Pizzuto, A. C. Walls, M. S. Diamond, A. Telenti, H. W. Virgin, A. Lanzavecchia, G. Snell, D. Veesler, D. Corti, Broadly neutralizing antibodies overcome SARS-CoV-2 Omicron antigenic shift. *Nature* **602**, 664–670 (2022).

48. Y. L. Cao, A. Yisimayi, F. C. Jian, W. L. Song, T. H. Xiao, L. Wang, S. Du, J. Wang, Q. Q. Li, X. S. Chen, Y. L. Yu, P. Wang, Z. Y. Zhang, P. L. Liu, R. An, X. H. Hao, Y. Wang, R. Feng, H. Y. Sun, L. J. Zhao, W. Zhang, D. Zhao, J. Zheng, L. L. Yu, C. Li, N. Zhang, R. Wang, X. Niu, S. J. Yang, X. T. Song, Y. Y. Chai, Y. Hu, Y. S. Shi, L. L. Zheng, Z. Q. Li, Q. Q. Gu, F. Shao, W. J. Huang, R. H. Jin, Z. Y. Shen, Y. C. Wang, X. X. Wang, J. Y. Xiao, X. S. Xie, BA.2.12.1, BA.4 and BA.5 escape antibodies elicited by Omicron infection. *Nature* **608**, 593–602 (2022).

49. D. Planas, N. Saunders, P. Maes, F. Guivel-Benhassine, C. Planchais, J. Buchrieser, W. H. Bolland, F. Porrot, I. Staropoli, F. Lemoine, H. Pere, D. Veyer, J. Puech, J. Rodary, G. Baele, S. Dellicour, J. Raymenants, S. Gorissen, C. Geenen, B. Vanmechelen, T. Wawina-Bokalanga, J. Marti-Carreras, L. Cuypers, A. Seve, L. Hocqueloux, T. Prazuck, F. A. Rey, E. Simon-Loriere, T. Bruel, H. Mouquet, E. Andre, O. Schwartz, Considerable escape of SARS-CoV-2 Omicron to antibody neutralization. *Nature* **602**, 671–675 (2022).

50. C. Drosten, S. Gunther, W. Preiser, S. van der Werf, H. R. Brodt, S. Becker, H. Rabenau, M. Panning, L. Kolesnikova, R. A. M. Fouchier, A. Berger, A. M. Burguiere, J. Cinatl, M. Eickmann, N. Escriou, K. Grywna, S. Kramme, J. C. Manuguerra, S. Muller, V. Rickerts, M. Sturmer, S. Vieth, H. D. Klenk, A. D. M. E. Osterhaus, H. Schmitz, H. W. Doerr, Identification of a novel coronavirus in patients with severe acute respiratory syndrome. *N. Engl. J. Med.* **348**, 1967–1976 (2003).

51. M. A. Tortorici, D. Veesler, Structural insights into coronavirus entry. *Adv. Virus Res.* **105**, 93–116 (2019).

52. V. D. Menachery, B. L. Yount, A. C. Sims, K. Debbink, S. S. Agnihothram, L. E. Gralinski, R. L. Graham, T. Scobey, J. A. Plante, S. R. Royal, J. Swanstrom, T. P. Sheahan, R. J. Pickles, D. Corti, S. H. Randell, A. Lanzavecchia, W. A. Marasco, R. S. Baric, SARS-like WIV1-CoV poised for human emergence. *Proc. Natl. Acad. Sci. U.S.A.* **113**, 3048–3053 (2016).

53. X. Y. Ge, J. L. Li, X. L. Yang, A. A. Chmura, G. J. Zhu, J. H. Epstein, J. K. Mazet, B. Hu, W. Zhang, C. Peng, Y. J. Zhang, C. M. Luo, B. Tan, N. Wang, Y. Zhu, G. Crameri, S. Y. Zhang, L. F. Wang, P. Daszak, Z. L. Shi, Isolation and characterization of a bat SARS-like coronavirus that uses the ACE2 receptor. *Nature* **503**, 535–538 (2013).

54. M. F. Boni, P. Lemey, X. W. Jiang, T. T. Y. Lam, B. W. Perry, T. A. Castoe, A. Rambaut, D. L. Robertson, Evolutionary origins of the SARS-CoV-2 sarbecovirus lineage responsible for the COVID-19 pandemic. *Nat. Microbiol.* **5**, 1408–1417 (2020).

55. C. Dacon, C. Tucker, L. Peng, C. D. Lee, T. H. Lin, M. Yuan, Y. Cong, L. Wang, L. Purser, J. K. Williams, C. W. Pyo, I. Kosik, Z. Hu, M. Zhao, D. Mohan, A. J. R. Cooper, M. Peterson, J. Skinner, S. Dixit, E. Kollins, L. Huzella, D. Perry, R. Byrum, S. Lembirik, D. Drawbaugh, B. Eaton, Y. Zhang, E. S. Yang, M. Chen, K. Leung, R. S. Weinberg, A. Pegu, D. E. Geraghty, E. Davidson, I. Douagi, S. Moir, J. W. Yewdell, C. Schmaljohn, P. D. Crompton, D. Nemazee, J. R. Mascola, I. A. Wilson, J. Tan, Broadly neutralizing antibodies target the coronavirus fusion peptide. *Science* **377**, 728–735 (2022).

56. J. S. Low, J. Jerak, M. A. Tortorici, M. McCallum, D. Pinto, A. Cassotta, M. Foglierini, F. Mele, R. Abdelnabi, B. Weynand, J. Noack, M. Montiel-Ruiz, S. Bianchi, F. Benigni, N. Sprugasci, A. Joshi, J. E. Bowen, C. Stewart, M. Rexhepaj, A. C. Walls, D. Jarrossay, D. Morone, P. Paparoditis, C. Garzoni, P. Ferrari, A. Ceschi, J. Neyts, L. A. Purcell, G. Snell, D. Corti, A. Lanzavecchia, D. Veesler, F. Sallusto, ACE2-binding exposes the SARS-CoV-2 fusion peptide to broadly neutralizing coronavirus antibodies. *Science* **377**, 735–742 (2022).

57. D. Pinto, M. M. Sauer, N. Czudnochowski, J. S. Low, M. A. Tortorici, M. P. Housley, J. Noack, A. C. Walls, J. E. Bowen, B. Guarino, L. E. Rosen, J. di Iulio, J. Jerak, H. Kaiser, S. Islam, S. Jaconi, N. Sprugasci, K. Culap, R. Abdelnabi, C. Foo, L. Coelmont, I. Bartha, S. Bianchi, C. Silacci-Fregni, J. Bassi, R. Marzi, E. Vetti, A. Cassotta, A. Ceschi, P. Ferrari, P. E. Cippa, O. Giannini, S. Ceruti, C. Garzoni, A. Riva, F. Benigni, E. Cameroni, L. Piccoli, M. S. Pizzuto, M. Smithey, D. Hong, A. Telenti, F. A. Lempp, J. Neyts, C. Havenar-Daughton, A. Lanzavecchia, F. Sallusto, G. Snell, H. W. Virgin, M. Beltramello, D. Corti, D. Veesler, Broad betacoronavirus neutralization by a stem helix-specific human antibody. *Science* **373**, 1109–1116 (2021).

58. K. H. Dinnon, S. R. Leist, A. Schafer, C. E. Edwards, D. R. Martinez, S. A. Montgomery, A. West, B. L. Yount, Y. X. J. Hou, L. E. Adams, K. L. Gully, A. J. Brown, E. Huang, M. D. Bryant, I. C. Choong, J. S. Glenn, L. E. Gralinski, T. P. Sheahan, R. S. Baric, A mouse-adapted model of SARS-CoV-2 to test COVID-19 countermeasures. *Nature* **586**, 560–566 (2020).

59. M. Superson, K. Szmyt, K. Szymańska, K. Walczak, J. Wnorowski, Ł. Zarębski, Clinical application of monoclonal antibodies in targeted therapy. *Eur J. Clin. Exp. Med.* **17**, 338–346 (2020).

60. C. Sundling, G. Phad, I. Douagi, M. Navis, G. B. K. Hedestam, Isolation of antibody V(D)J sequences from single cell sorted rhesus macaque B cells. *J. Immunol. Methods* **386**, 85–93 (2012).

61. K. Wiehe, D. Easterhoff, K. Luo, N. I. Nicely, T. Bradley, F. H. Jaeger, S. M. Dennison, R. Zhang, K. E. Lloyd, C. Stolarchuk, R. Parks, L. L. Sutherland, R. M. Scearce, L. Morris, J. Kaewkungwal, S. Nitayaphan, P. Pitisuttithum, S. Rerks-Ngarm, F. Sinangil, S. Phogat, N. L. Michael, J. H. Kim, G. Kelsoe, D. C. Montefiori, G. D. Tomaras, M. Bonsignori, S. Santra, T. B. Kepler, S. M. Alam, M. A. Moody, H.-X. Liao, B. F. Haynes, Antibody light-chain-restricted recognition of the site of immune pressure in the RV144 HIV-1 vaccine trial is phylogenetically conserved. *Immunity* **41**, 909–918 (2014).

62. S. Ravichandran, J. Tang, G. Grubbs, Y. Lee, S. Pourhashemi, L. Hussaini, S. A. Lapp, R. C. Jerris, V. Singh, A. Chahroudi, E. J. Anderson, C. A. Rostad, S. Khurana, SARS-CoV-2 immune repertoire in MIS-C and pediatric COVID-19. *Nat. Immunol.* **22**, 1452–1464 (2021).

63. J. Tang, T. Novak, J. Hecker, G. Grubbs, F. T. Zahra, L. Bellusci, S. Pourhashemi, J. Chou, K. Moffitt, N. B. Halasa, S. P. Schwartz, T. C. Walker, K. M. Tarquinio, M. S. Zinter, M. A. Staat, S. J. Gertz, N. Z. Cvijanovich, J. E. Schuster, L. L. Loftis, B. M. Coates, E. H. Mack, K. Irby, J. C. Fitzgerald, C. M. Rowan, M. Kong, H. R. Flori, A. B. Maddux, S. L. Shein, H. Crandall, J. R. Hume, C. V. Hobbs, A. H. Tremoulet, C. Shimizu, J. C. Burns, S. R. Chen, H. K. Moon, C. Lange, A. G. Randolph, S. Khurana, Cross-reactive immunity against the SARS-CoV-2 Omicron variant is low in pediatric patients with prior COVID-19 or MIS-C. *Nat. Commun.* **13**, 2979 (2022).

64. S. Ravichandran, E. M. Coyle, L. Klenow, J. Tang, G. Grubbs, S. Liu, T. Wang, H. Golding, S. Khurana, Antibody signature induced by SARS-CoV-2 spike protein immunogens in rabbits. *Sci. Transl. Med.* **12**, eabc3539 (2020).

65. F. T. Zahra, L. Bellusci, G. Grubbs, H. Golding, S. Khurana, Neutralisation of circulating SARS-CoV-2 delta and omicron variants by convalescent plasma and SARS-CoV-2 hyperimmune intravenous human immunoglobulins for treatment of COVID-19. *Ann. Rheum. Dis.* **81**, 1044–1045 (2022).

66. D. C. Ekiert, R. H. E. Friesen, G. Bhabha, T. Kwaks, M. Jongeneelen, W. Yu, C. Ophorst, F. Cox, H. J. W. M. Korse, B. Brandenburg, R. Vogels, J. P. J. Brakenhoff, R. Kompier, M. H. Koldijk, L. A. H. M. Cornelissen, L. M. Poon, M. Peiris, W. Koudstaal, I. A. Wilson, J. Goudsmit, A highly conserved neutralizing epitope on group 2 influenza A viruses. *Science* **333**, 843–850 (2011).

67. Z. Otwinowski, W. Minor, Processing of X-ray diffraction data collected in oscillation mode. *Methods Enzymol.* **276**, 307–326 (1997).

68. A. J. McCoy, R. W. Grosse-Kunstleve, P. D. Adams, M. D. Winn, L. C. Storoni, R. J. Read, Phaser crystallographic software. *J. Appl. Cryst.* **40**, 658–674 (2007).

69. P. Emsley, B. Lohkamp, W. G. Scott, K. Cowtan, Features and development of Coot. *Acta Crystallogr. D Biol. Crystallogr.* **66**, 486–501 (2010).

70. P. D. Adams, P. V. Afonine, G. Bunkoczi, V. B. Chen, I. W. Davis, N. Echols, J. J. Headd, L. W. Hung, G. J. Kapral, R. W. Grosse-Kunstleve, A. J. McCoy, N. W. Moriarty, R. Oeffner, R. J. Read, D. C. Richardson, J. S. Richardson, T. C. Terwilliger, P. H. Zwart, PHENIX: A comprehensive Python-based system for macromolecular structure solution. *Acta Crystallogr. D Biol. Crystallogr.* **66**, 213–221 (2010).

71. E. Krissinel, K. Henrick, Inference of macromolecular assemblies from crystalline state. *J. Mol. Biol.* **372**, 774–797 (2007).

72. F. Zhang, L. Wang, X. Niu, J. Li, J. Luo, Y. Feng, Y. Yang, P. He, W. Fan, R. Liang, Z. Zheng, W. Pan, C. Li, Y. Tan, H. Yu, L. Chen, P. Li, Phenotypic characterization of chinese rhesus macaque plasmablasts for cloning antigen-specific monoclonal antibodies. *Front. Immunol.* **10**, 2426 (2019).

73. V. B. Chen, W. B. Arendall III, J. J. Headd, D. A. Keedy, R. M. Immormino, G. J. Kapral, L. W. Murray, J. S. Richardson, D. C. Richardson, MolProbity: All-atom structure validation for macromolecular crystallography. *Acta Crystallogr. D Biol. Crystallogr.* **66**, 12–21 (2010).